Version of Record: https://www.sciencedirect.com/science/article/pii/S0924796317304219
Manuscript_f421aaa3a9e7b54d53fd5c039668301c

Anaerobic ammonium oxidation (anammox) and denitrification in Peru margin sediments

Jeremy J. Rich[1*], Philip Arevalo[2], Bonnie X. Chang[3], Allan H. Devol[4], and Bess B. Ward[5]

[1]School of Marine Sciences and Darling Marine Center, University of Maine, Walpole, Maine, 04573 USA

[2]Department of Ecology & Evolution, University of Chicago, Chicago, Illinois, 60637 USA

[3]Joint Institute for the Study of the Atmosphere and Ocean, University of Washington and NOAA/Pacific Marine Environmental Laboratory, Seattle, Washington, 98115

[4]School of Oceanography, University of Washington, Seattle, Washington, 98195 USA

[5]Department of Geosciences, Princeton University, Princeton, New Jersey, 08544 USA

*Corresponding author, jeremy.rich@maine.edu

Running title: Anammox in Peru margin sediments

© 2018 published by Elsevier. This manuscript is made available under the Elsevier user license
https://www.elsevier.com/open-access/userlicense/1.0/

Abstract

The upwelling system of coastal Peru supports very high primary production, contributing to an oxygen deficient zone (ODZ) in subsurface waters and high organic matter deposition rates to underlying sediments. Although anammox and denitrification have been relatively well studied in ODZ waters, few studies have investigated these processes in the underlying sediments. We sampled seven stations over a large geographic area along the Peru margin, spanning a water depth of 100-3240 m. At two of the central shelf stations (100 m and 325 m), we observed *Thioploca*, with a well-developed mat at the shallowest station (100 m). We measured sediment properties and conducted shipboard ^{15}N-incubations of homogenized sediments to determine potential rates of anammox and denitrification and potential controlling factors at each station. Diversity of anammox bacteria based on 16S rRNA and hydrazine oxidoreductase (*hzo*) sequences and *hzo* gene abundances were measured at each station. Overall, organic C content was high across the stations (3-12%), except for two of the deepest stations (~1.5%). Porewater ammonium fluxes and ammonium production rates in shipboard incubations, reflecting sediment organic carbon decomposition rates, were higher at the two central shelf stations compared to the other stations. The range in average potential rates was 2.1-80.4 nmol N cm^{-3} h^{-1} for denitrification and 1.8-44.2 nmol N cm^{-3} h^{-1} for anammox. The range in relative anammox (*ra*) across stations was 2.6-47.4%, with an average of 34.2%. The lowest *ra* was found at the shallowest shelf station with *Thioploca* mats and highest ammonium production rates. The *ra* jumped up to 45.9% at the station with the next highest ammonium production rates, corresponding to the deeper shelf station (325 m). At the other stations, *ra* was relatively high (39.6-47.4%), except at one station (16.3%), reflecting similar ammonium production rates due to decomposition across these stations. Anammox bacteria in the *Candidatus* Scalindua genus

47 were the only anammox bacteria detected in Peru margin sediments based on 16S rRNA or *hzo*
48 sequences. Copy number of *hzo* indicated abundant populations of anammox bacteria across the
49 stations. However, *hzo* copy number did not correlate with anammox rates or *ra*. Overall, our
50 results suggest that anammox contributes significantly to N_2 production in Peru margin
51 sediments, except in shelf sediments with high decomposition rates and dense *Thioploca* mats.
52

1.0. Introduction

Nitrogen is the macronutrient most often limiting primary productivity in marine ecosystems. Therefore, processes that control the fate and abundance of nitrogen are critical to ecosystem functioning. Denitrification is the step-wise reduction of NO_3^- to N_2, coupled to the oxidation of organic carbon, H_2, reduced sulfur, or ferrous iron, under anoxic conditions. Denitrification is carried out by a diverse polyphyletic group of bacteria and some archaea, including phototrophic, chemolithotrophic, and heterotrophic organisms and even eukaryotes, such as foraminifera (Risgaard-Petersen et al. 2006, Zumft 1997). Anaerobic ammonium oxidation (anammox) is the oxidation of NH_4^+, with NO_2^-, in the absence of O_2 to form N_2. Anammox is carried out by a monophyletic group of *Planctomycetes*. Although anammox bacteria can oxidize organic acids, they grow primarily as autotrophs (Kartal et al. 2011a). It has long been assumed that denitrification was the dominant process producing N_2 under anoxic conditions in natural ecosystems. It is now clear, however, that anammox is an important alternative pathway of N_2 production in the global nitrogen cycle. Information regarding the relationship between anammox and denitrification in terms of N_2 production is critical for understanding the global nitrogen cycle.

An important sink in global N budgets occurs in the water column of the major oxygen deficient zones (ODZs), located in the Eastern Tropical North and South Pacific and in the Arabian Sea (Galloway et al. 2004). The relative contribution of anammox and denitrification to N_2 flux in these regions has received considerable attention, and either anammox or denitrification contributes substantially to N_2 production, depending on timing and location, while overall the contribution of anammox is likely to be limited by stoichiometric constraints (Dalsgaard et al. 2012, Lam et al. 2009, Ward et al. 2009, Babbin et al. 2014). However,

uncertainties about which process dominates at any given location or time, indicate that factors controlling the relative contribution of each process are still not adequately understood. An even larger N sink occurs in ocean sediments, particularly continental shelf and slope sediments, and possibly deep-sea sediments. A number of studies of denitrification in marine sediments exist, especially in shelf sediments, and denitrification has been modeled in deep-sea sediments (e.g., Christensen et al. 1987, Devol 1991, and Middelburg et al. 1996). Thamdrup and Dalsgaard (2002) first demonstrated that anammox accounted for up to 67% of N_2 production in sediments from the Skagerrak, with the remaining N_2 resulting from denitrification. The experiments conducted by Thamdrup and Dalsgaard (2002) were based on incubations of homogenized sediments amended with $^{15}NO_3^-$ and are generally referred to as isotope pairing experiments, building off earlier work (Nielsen 1992). The relative contribution of anammox to the total N_2 production rate in these types of incubations is referred to as *ra* (i.e., *ra*=100[(anammox rate)/(anammox rate+denitrification rate]; Trimmer and Engström et al. 2011). Engström et al. (2005) found somewhat higher *ra* (79%) at some of the same sites sampled by Thamdrup and Dalsgaard (2002) in the Skagerrek. In both studies, *ra* increased with depth due to lower rates of denitrification linked to lower rates of overall organic C decomposition rates with water depth, while anammox rates were relatively more constant than denitrification rates. This suggested that flux of labile organic carbon was one of the primary factors controlling *ra*, as driven primarily by changes in rates of denitrification rather than anammox. Since the original work in the Skagerrak, many more studies have measured anammox and denitrification potential rates, confirming that *ra* is generally low in shallow coastal sediments (Trimmer and Engström 2011). Measurements in deep-sea sediments are less common, but the measurements that have been

made confirm that *ra* is higher in deeper sediments compared to coastal sediments, although there are exceptions (Trimmer and Nichols 2009, Engström et al. 2009, and Sokoll et al. 2012).

At least five genera of anammox bacteria have been identified thus far, including *Candidatus* Brocadia, Kuenenia, and Scalindua, which together form a deeply branching group of *Planctomycetes*, based on 16S rRNA gene sequences (Kartal et al. 2011a). A variety of environments have been examined for 16S rRNA genes specific for anammox bacteria, and *Ca.* Scalindua is the only genus usually detected in marine environments (Sonthiphand et al. 2014). Hydrazine is an intermediate in the anammox reaction, and hydrazine oxidoreductase (Hzo) has been identified as a key enzyme in the pathway, oxidizing hydrazine to N_2 (Kartal et al. 2011b). Hzo is in the octaheme cytochrome hydroxylamine oxidoreductase (Hao) family of proteins, of which several divergent octaheme protein coding sequences are found in anammox bacteria. In the Kuenenia genome, there are two copies of nearly identical Hzo sequences corresponding to functional proteins responsible for hydrazine oxidation to N_2. These two protein sequences form a specific phylogenetic cluster distinct from other putative Hzo/Hao proteins (Kartal and Keltjens 2016, Klotz et al. 2008, Schmid et al. 2008). PCR primers have been developed to detect the gene sequences corresponding to the two functional Hzo proteins, thereby serving as a biomarker of anammox bacteria in the environment (Hirsch et al. 2011, Schmid et al. 2008).

The water column off Peru is characterized by high primary productivity and a large ODZ, with high rates of organic matter deposition to underlying sediments (Froelich et al. 1988, Hedges and Keil 1995, Henrichs and Farrington 1984, Levin et al. 2002). The Peruvian ODZ occurs at water depth of ~20-500 m. As such, shelf sediments are covered by anoxic water conducive to the growth of *Thioploca* bacteria that can form thick fibrous mats at certain locations (Fossing et al. 1995, Schulz et al. 1996). *Thioploca* store up to 550 mM NO_3^- in

121 internal vacuoles and they respire NO_3^- to NH_4^+, rather than N_2, in the process known as
122 dissimilatory nitrate reduction to ammonium (DNRA), with reduced sulfur as an electron donor
123 (Otte et al. 1999). Anammox bacteria have been shown to form specific associations with
124 *Thioploca* filaments, as *Thioploca* can produce both substrates needed in the anammox reaction
125 (Prokopenko et al. 2013). However, based on simulation models of measured solute fluxes,
126 anammox rates were relatively low compared to denitrification in sediments with *Thioploca* mats
127 on the Peruvian shelf (Bohlen et al. 2011). Furthermore, foraminifera contain very high
128 concentrations of intracellular NO_3^-, as well, and could theoretically account for a significant
129 portion of denitrification in Peru margin sediments (Glock et al. 2013). Release or mixing of
130 intracellular $^{14}NO_3^-$ from *Thioploca* or foraminifera in sediment incubations with added $^{15}NO_3^-$
131 has the potential to lead to significant overestimates of anammox rates, if intracellular $^{14}NO_3^-$ is
132 not adequately accounted for (Sokoll et al. 2012 and Song et al. 2013). DNRA produces $^{15}NH_4^+$
133 from added $^{15}NO_3^-$ that can then combine with $^{15}NO_2^-$, leading to an underestimate of anammox
134 rates (Song et al. 2013 and Song et al. 2016). As significant intracellular NO_3^- and DNRA would
135 be expected to occur at some locations in Peru margin sediments, modifications to the standard
136 isotope pairing method would be necessary to determine anammox and denitrification rates in
137 these situations (Sokoll et al. 2012, Song et al. 2013, and Song et al. 2016).
138 In the current study, we used the ^{15}N-isotope pairing technique to measure potential rates
139 of anammox and denitrification in homogenized sediments from seven stations in the Peru
140 margin that spanned a water depth of 100-3250 m. We also measured the diversity of anammox
141 specific 16S rRNA and *hzo* sequences, and the abundance of *hzo* genes using quantitative PCR at
142 the same stations. Our objectives were to provide the first direct measurements of anammox and
143 denitrification potential rates in Peru margin sediments using isotope pairing, thereby providing

144 further insights into processes that may regulate anammox in marine sediments and the potential
145 significance of anammox as a nitrogen loss pathway in the Peru margin sediments.
146
147 **2.0. Methods**
148 *2.1 Sample locations and site characteristics*
149 A multi-corer (Ocean Instruments, MC-800) was used to obtain intact surface sediments at seven
150 stations in the Peru margin, aboard the R/V Knorr in October 2005 (leg 182-9) (Fig. 1, Table 1).
151 Bottom water temperature was measured with the CTD (Sea-Bird Electronics, SBE9) and
152 dissolved O_2 of the water column was measured using a probe (Sea-Bird Electronics, SBE43;
153 detection limit ~2 µM) mounted on the CTD, calibrated with the micro-Winkler technique
154 (Broenkow and Cline 1969). NO_3^- and NO_2^- in the bottom water were measured with sensitivities
155 of ± 0.1 µM for NO_3^- and ± 0.01 µM for NO_2^- using standard techniques (Braman and Hendrix
156 1989, Strickland and Parsons 1972). The percent of total organic carbon (%TOC) in the top 0-1
157 cm of sediment collected in one of the multi-core tubes at each station was measured in acidified
158 sediment samples with an elemental analyzer (Carlo Erba Model 1108).
159
160 *2.2 Potential anammox and denitrification rates*
161 The sediment processing, incubation conditions, ^{15}N additions, and analytical measurements
162 were conducted following previously published methods (Rich et al. 2008, Risgaard-Petersen et
163 al. 2004, Thamdrup and Dalsgaard 2002). Briefly, where bottom waters contained measureable
164 O_2, the oxygen penetration depth was measured with a Clark type microelectrode. Sediments just
165 below the oxygen penetration depth or the top layer of sediment when cores were collected in the
166 ODZ were sectioned (2 cm depth interval) and immediately transferred to an N_2 flushed glove

bag, where the sediment was homogenized and transferred to vials (1.5 ml sediment slurry in 5.9 ml Exetainer vials). The vials were sealed and removed from the glove bag, flushed with He, and pre-incubated for 1-3 h at the incubation temperature of 12°C, such that rates were obtained at the same temperature across stations. Tracer and carrier solutions were purged with helium and manipulated using helium-purged gas-tight glass syringes. Vials were injected with either $^{15}NO_3^-$ $+^{14}NH_4^+$, $^{15}NH_4^+$, or $^{14}NO_3^-+^{15}NH_4^+$ (100 nmol N cm^{-3} sediment) after the preincubation period and triplicate vials were killed at various time points with $ZnCl_2$ (100µl 7M) during 8-16 h incubations. The ^{15}N content of the resulting N_2 was determined by isotope ratio mass spectrometry using a Europa 20/20.

In incubations with added $^{15}NO_3^-+^{14}NH_4^+$, the fraction of $NO_3^-+NO_2^-$ as ^{15}N (F_n) was determined by difference, before and immediately after $^{15}NO_3^-$ addition, accounting for the atom% of the stock solution, except at the two central shelf stations with visible *Thioploca* (100 m and 325 m) (see below). The rates of $^{15}N^{14}N$ and $^{15}N^{15}N$ production from added $^{15}NO_3^-$ and F_n were used in the equations of Thamdrup and Dalsgaard (2002) to calculate potential rates of anammox and denitrification. In incubations that received additions of $^{15}NH_4^+ + ^{14}NO_3^-$, the anammox rate was calculated using the following equation, as modified from a previous study (Thamdrup and Dalsgaard 2000): $dN_2/dt = d^{29}N_2/dt \times F_a^{-1}$, where $F_a = (f_0+f_t)/2$, f_0 = fraction of NH_4^+ that was labeled with ^{15}N at time zero, and f_t = fraction of NH_4^+ that was labeled with ^{15}N at the end of interval t, in which the rate was determined. This was to account for any change in F_a during the course of incubations due to release of $^{14}NH_4^+$ during organic matter decomposition or conversion of added $^{14}NO_3^-$ to $^{14}NH_4^+$ by DNRA. The f_0 was determined by difference, before and immediately after $^{15}NH_4^+$ addition, accounting for the atom% of the stock solution and NH_4^+ in the porewater and adsorbed to sediment colloids, as determined by the

recovery of added NH_4^+ in the porewater (Thamdrup and Dalsgaard 2000). The f_t was calculated according to the following equation: $f_t = ([^{15}NH_4^+{}_{t0}]-0.5A29)/(\Sigma NH_4^+{}_t)$, where *A29* is the amount of $^{15}N^{14}N$ produced in the time interval *t* and $\Sigma NH_4^+{}_t$ is the measured NH_4^+ concentration at *t*. Rates were based on difference between the first and second time points as rates leveled off after the second time point in sediment incubations due to complete consumption of added NO_3^- in three of seven stations. In sediments where *Thioploca* sheaths were observed (i.e., 100 m and 325 m), high and variable initial NO_3^- concentrations were measured in unamended sediment slurries, reflecting release of intracellular NO_3^- during sample processing (e.g., Thamdrup and Canfield 1996). To address this issue, it was assumed that anammox rates in sediments where *Thioploca* sheaths were observe were equivalent in either $^{15}NO_3^-+^{14}NH_4^+$ or $^{15}NH_4^++^{14}NO_3^-$ additions (Sokoll et al. 2012; Song et al. 2013). This was assumed as anammox rates were equivalent in the two different isotope additions in sediment samples without *Thioploca*. This enabled F_n to be calculated in incubations with added $^{15}NO_3^-+^{14}NH_4^+$ based on the anammox rate determined in the $^{15}NH_4^++^{14}NO_3^-$ additions and measured $^{15}N^{14}N$ and $^{15}N^{15}N$ production in $^{15}NO_3^-+^{14}NH_4^+$ additions.

2.3. Porewater depth profiles and ammonium production

Concentration of $NO_3^-+NO_2^-$ and NH_4^+ were measured in porewater depth profiles collected at five of the seven stations using sediment from one of the multi-core tubes at each station. The sediment from the core tube was sectioned in 0.5-1.0 cm intervals, centrifuged, and the supernatant was filtered through 0.45 μm filters (profiles from MC2 and MC9 were not determined). Porewaters were frozen until analyzed for $NO_3^-+NO_2^-$ and NH_4^+ following previously published methods (Koroleff 1983; analytical error for $NO_3^-+NO_2^-$ was ± 0.1 μM and

213 for NH_4^+ was ± 0.3 µM). A form of Fick's first law was used to calculate the diffusive flux (*J*) of
214 NO_3^-+NO_2^- and NH_4^+, $J = \phi D_s(\delta C/\delta z)$, where $(\delta C/\delta z)$ is the steepest measured concentration
215 gradient, ϕ is the porosity, and D_s is the sediment diffusion coefficient. The sediment diffusion
216 coefficient, D_s, was calculated as the product of the molecular diffusion coefficient and the
217 porosity (Ullman and Aller, 1982). The molecular diffusion coefficients of NO_3^-+NO_2^- (D_{nt}) and
218 NH_4^+ (D_a) were calculated at the appropriate bottom water temperature using the equations
219 according to Boudreau (1997), $D_{nt} = (9.5 + 0.388T)10^{-6}$ and $D_a = (9.5 + 0.413T)10^{-6}$, where T is
220 temperature in degrees Celsius.
221 In the same laboratory incubations that were used to determine anammox and
222 denitrification potential rates, the production rate of dissolved NH_4^+ was determined after NO_3^-
223 was consumed, which would reflect NH_4^+ production from decomposing organic matter as a
224 proxy for flux of labile organic C across sites. As NO_3^- was always present during the incubation
225 from the deepest station (MC15), NH_4^+ loss due to anammox during the incubation was
226 accounted for in the NH_4^+ production rate determined at this station (i.e., $P_a = d[NH_4^+]/dt +$
227 $0.5A$, where P_a = NH_4^+ production rate, and A = anammox rate).
228
229 *2.4. Diversity and phylogenetic analyses of anammox specific 16S rRNA and hzo genes*
230 Six sub-samples (0.5 ml) of the homogenized sediment slurry from each station were flash
231 frozen in liquid N_2 and transported back to the laboratory. Total DNA was extracted using the
232 MoBio PowerSoil DNA Isolation kit and quantified on a Qubit Fluorometer (Invitrogen).
233 Extracts were diluted to a final concentration of 10 ng DNA μl^{-1} and duplicate extracts were
234 pooled, resulting in three replicate DNA extracts per site. The *Planctomycete*-specific primer
235 Pla46 (5'-GGATTAGGCATGCAAGTC-3') (Neef et al. 1998) and the anammox-specific primer

BS820R (5'-TAATTCCCTCTACTTAGTGCCC-3') (Kuypers et al. 2003) were used to amplify a 807 bp fragment of the 16S rRNA gene (Schmid et al. 2005), and primers hzocl-f1 (5'-TGYAAGACYTGYCAYTGG-3') and hzocl-r2 (5'-ACTCCAGATRTGCTGACC-3') were used to amplify a 471 bp fragment of the anammox-specific gene hydrazine oxidoreductase (*hzo*) (Schmid et al. 2008), using the following reaction conditions: 40 ng template DNA, 0.2 mM dNTP, 0.064% BSA, 0.03 units μl^{-1} GoTaq HotStart Polymerase (Promega), 0.4 μM forward primer, 0.4 μM reverse primer, 1x GoTaq Flexi Buffer (Promega), and a final reaction volume of 20 μl. After an initial denaturation at 94°C for 5 minutes the following cycle was repeated 30 times: denaturation at 94°C for 60 s, 60 annealing at 56°C for 60 s, and extension at 72°C for 90 s. After the final cycle, a 10 minute final extension step was performed at 72°C. PCR products were run on a 1.5% agarose gel and visualized under UV light with 1.5% ethidium bromide. Fragment bands of the appropriate size were excised from gels and the DNA was extracted using the QIAquick Gel Extraction Kit (Qiagen). PCR products were ligated into the pGEM-T vector (Promega) and transformations were performed according to the manufacturer's instructions. Approximately 20 clones with inserts for each gene, from each station, were selected at random for sequencing using the Sanger method (Genetic Analyzer 3500, Applied Biosystems). The *hzo* nucleotide and amino acid sequences were aligned in muscle (Schloss et al. 2009), and the final alignment for amino acid sequences was 145 residues and for nucleotide sequences was 435 bp. The 16S rDNA sequences were aligned in NAST as implemented on the greengenes website, and the final alignment was 768 bp (DeSantis et al. 2006). The16S rDNA operational taxonomic units (OTUs) were grouped at the 98% similarity level, *hzo* nucleotides sequences at the 96% similarity level, and amino acid sequences at the 99% similarity level using the farthest neighbor method as implemented in mothur (Schloss et al. 2009). Maximum-likelihood phylogenetic trees

were generated on the PhyML online platform with one hundred bootstrap replicates (Guindon et al. 2010).

2.5. hzo gene abundance

For quantitative PCR, the Primer3 program was used to design suitable forward and reverse primers based on the 112 *hzo* sequences generated in this study, specifying a product of between 100-200 bp in length (Rozen and Skaletsky 1999). The derived forward (hzo-qf; 5'-CACAAGTATGGGTATGTCAAATGC-3') and reverse (hzo-qr, 5'-TTGCAAACCTTGGTGAATG-3') primers amplified a 106 bp *hzo* fragment and were a perfect match for 97 of the 112 *hzo* sequences generated in this study, with one or two mismatches for the remaining sequences. Triplicate DNA extracts from each station were subjected to qPCR using the following conditions: 1x Phusion Flash enzyme master mix (Finnzymes), 1x SYBR green (Invitrogen), 0.5 μM forward primer, 0.5 μM reverse primer, 2 ng template DNA, and a final reaction volume of 20 μl. Reactions were performed on TwinTec Realtime 96-well white PCR plates on the Mastercycler Realplex thermal cycler (Eppendorf). After an initial 10 s denaturation step at 98°C, the following cycle was repeated 40 times: 98°C denaturation for 1 s, 58°C annealing for 5 s, and 72°C extension for 8s with a hold for plate reading. Linearized plasmids containing a known copy number of *hzo* were used to generate standard curves.

2.6. Accession numbers

Gene sequences were submitted to Genbank on under accession numbers JQ308954-JQ309035 for 16S rRNA and AFF59692-AFF59803 for *hzo*.

3.0 Results

3.1 Station and sediment characteristics

The sample locations were distributed over a broad area along the Peru margin, spanning a water depth of 100-3240 m (Figure 1, Table 1). There was one shelf station along the thin shelf section of southern Peru and two shelf stations in the broader shelf area of central Peru, with O_2 concentrations in the bottom water at or below the detection limit and high NO_2^- concentrations. The three slope stations were in the central or southern areas of the study region and had an O_2 concentration of 65-72 µM in the overlying water. The rise station was off northern Peru and had an O_2 concentration of 112 µM in the overlying water. Since O_2 at the shelf stations was at or below detection, oxygen penetration depth in these sediments was not measured. The range in O_2 penetration in slope sediments was 0.5-0.8 cm, while O_2 penetration at the rise station was 1.5 cm (Table 2). Across stations, the range in %TOC was 1.5-12.5%, with the highest %TOC (>7%) at the two central shelf stations and one of the slope stations. At the two central shelf stations, *Thioploca* was visually observed in multi-cores, with a dense mat of *Thioploca* at the shallowest station, 100 m, and low density *Thioploca* mat with sparse filaments at 325 m.

3.2. Porewater depth profiles

$NO_3^-+NO_2^-$ concentrations were significantly higher in the porewater of surface sediments of the central shelf stations, reflecting release of intracellular NO_3^- during centrifugation of sediment slices, presumably due to disturbance of *Thioploca* during sample processing (Figure 2) Meanwhile $NO_3^-+NO_2^-$ profiles for the slope and rise stations did not appear influenced by any release of intracellular NO_3^-, and downward $NO_3^-+NO_2^-$ fluxes at these stations were determined based on porewater profiles (Table 2). The porewater NH_4^+ concentration was higher in surface

sediments at the central shelf stations compared to the slope and rise stations, and had correspondingly higher upward NH_4^+ fluxes. There was a slight increase in NH_4^+ in the surface layer at 940 m and 3240 m stations, presumably reflecting cell lysis during core retrieval in the surface layer of these sediments (Berelson et al. 1990; Haeckel et al. 2001), which overall had lower NH_4^+ concentrations throughout the profile. The increase in surface NH_4^+ should not influence calculated NH_4^+ fluxes as the flux calculations are based on the steepest gradient below the surface increase in NH_4^+. Downward NO_3^-+NO_2^- fluxes were higher than upward NH_4^+ fluxes at the three stations where it was possible to make a comparison. At these three stations, assuming that all of the upward NH_4^+ flux was consumed by anammox, and all of the downward flux of NO_3^-+NO_2^- was converted to N_2 either by denitrification or anammox, the range in percent of N_2 production attributed to anammox was 12-44% (Table 2). Note that this calculation does not take into account the possibility of nitrification occurring at very low O_2 concentrations (Bristow et al. 2016).

3.3. ^{15}N-sediment incubations

When NO_3^- or NO_2^- disappeared in incubations of homogenized sediments, ^{15}N-N_2 production ceased (Figures 3 and 4). $^{15}N^{14}N$ production exceeded or was similar to that of $^{15}N^{15}N$ in sediments with added $^{15}NO_3^-$+$^{14}NH_4^+$, except 940 m where $^{15}N^{15}N$ was higher than $^{15}N^{14}N$ production (second from top row, Figures 3 and 4). In sediments with added $^{15}NH_4^+$ only or $^{15}NH_4^+$+$^{14}NO_3^-$, $^{15}N^{15}N$ production was not detected in any of the sediments (bottom two rows, Fig. 3 and 4). In sediments with added $^{15}NH_4^+$+$^{14}NO_3^-$, significant $^{15}N^{14}N$ production was detected in all the sediments, except 100 m (bottom row, Figures 3 and 4). The total accumulation of $^{15}N^{14}N$ was higher in sediments with added $^{15}NH_4^+$+$^{14}NO_3^-$ than in sediments

with added $^{15}NH_4^+$ only, except in 100 m station samples where $^{15}N^{14}N$ was very low or not detected in either treatment (compare bottom two rows, Figures 3 and 4). $^{15}N^{14}N$ production in the presence of $^{15}NH_4^+$ alone reflected the concentration of NO_3^-+NO_2^- that was present in the vials at the end of 1-3 h preincubations and levels of anammox rates in samples. At the 100 m station there was ~100 nmol N cm^{-3} of NO_3^-+NO_2^- present after the pre-incubation step but very low or no production of $^{15}N^{14}N$ in either $^{15}NH_4^+$+$^{14}NO_3^-$ or $^{15}NH_4^+$ only treatments, indicating low anammox rates at the 100 m station. In samples from the 940 m station there was the lowest concentration of NO_3^-+NO_2^- present (<1 nmol N cm^{-3}) after the preincubation step among the stations and $^{15}N^{14}N$ production was not detected in these samples with added $^{15}NH_4^+$ only.

There was significant release of intracellular NO_3^- in incubations with sediments from the central shelf stations (100 m and 325 m stations). Therefore, we relied on only one of the isotope additions (i.e., $^{15}NH_4^+$+$^{14}NO_3^-$ additions) to determine anammox rates at the 100 m and 325 m stations. At the other five stations, we were able to determine anammox rates based on either isotope addition (i.e., $^{15}NH_4^+$+$^{14}NO_3^-$ and $^{15}NO_3^-$+$^{14}NH_4^+$). At these five stations, there was agreement in anammox rates between the two combinations of isotope additions, with a positive correlation and slope not significantly different from one across five stations (Figure 5).

The range in average rates across stations was 1.8-44.2 nmol N cm^{-3} h^{-1} for anammox and 2.1-80.4 nmol N cm^{-3} h^{-1} for denitrification (Table 3, Figure 6C). Except for the shallowest station (100 m), anammox potential rates decreased with depth. Denitrification potential rates also decreased with depth, with the exception of the 930 m station. Denitrification potential rates decreased more than anammox potential rates with depth. The range in *ra* was 2.6-47.4% across stations, with an average of 34.2%. Excluding the 100 m and 930 m stations, *ra* was similar (i.e., ~40-47%) at stations with very different depths (120-3240 m), indicating that anammox and

denitrification potential rates changed similarly with depth at these stations. As a proxy of organic C decomposition rates and therefore availability of labile C, we relied on NH_4^+ flux rates from porewater depth profiles and NH_4^+ production in ^{15}N incubations corresponding to the part of the incubation after NO_3^- had been consumed or in the case of the 3240 m station during the period that NO_3^- was present, as NO_3^- was never completely consumed during the incubation at the 3240 m station. In five out of seven stations, it was possible to compare trends in these two proxies, and the trends generally agreed at these five stations (100 m, 325 m, 940 m, 1460 m, and 3240 m), with highest NH_4^+ production at the two central shelf stations (Figure 6B). NH_4^+ production rates in vials did not follow a consistent decrease with depth with similar rates across a depth range of 120-3240 m, with the exception in this depth range at the 325 m station.

3.4. Anammox specific 16S rRNA and hzo diversity and hzo gene abundance

A total of 112 clones were sequenced from seven 16S rRNA libraries, corresponding to each station. Based on BLAST and phylogenetic analyses, 30 16S rRNA sequences fell outside the anammox-specific cluster and were excluded from further analyses. The remaining 82 sequences had high identity with sequences in the *Candidatus* Scalindua group (Figure 7). These sequences formed 19 OTUs at the 98% similarity level. A total of 112 *hzo* clones were also sequenced from seven libraries, corresponding to each station. All of the *hzo* sequences had high identity with *Ca.* Scalindua. The *hzo* nucleotide sequences formed 22 OTUs at the 96% similarity level.

Eight OTUs were deduced from the Hzo amino acid sequences at the 99% similarity level. The two most abundant OTUs (PMHA-1 and PMHA-6) contained 92% of all sequenced clones in the same subcluster in phylogenetic trees (Figure 8). Although these two sequence types differed by only one amino acid substitution, their relative abundance in clone libraries

appeared related to water column depth, with PMHA-1 in greater abundance in shelf sediments than deeper stations, and the opposite trend for PMHA-6 (Figure 6D). When aligned with the full-length Kuenenia sequence (CAJ71439), the change occurred at amino acid position 415, one residue from a putative heme binding motif, CDDCH at positions 416-420 (Schmid et al. 2008). The shallower station sequence (PMHA-1) has an alanine and the deeper station sequence (PMHA-6) has a valine at position 415.

The range in average *hzo* gene abundance across stations was 5.6×10^6-1.5×10^8 copies cm^{-3} sediment, with the lowest values at the deepest station (3240 m) and highest at the 325 m station (Table 3, Figure 6A). The other five stations had similar average *hzo* abundance of about 5×10^7 copies cm^{-3} sediment. Average *hzo* gene abundance did not correlate significantly with potential anammox rates or *ra* across stations.

4.0 Discussion

4.1 Importance of denitrification and anammox as N loss pathways in marine sediments

In this study, rates of anammox and denitrification were determined in shipboard laboratory incubations of homogenized sediments with substrate concentrations that were not limiting. As such, the rates reported in this study are potential rates and therefore we have not extrapolated these rates to regional estimates of the total sediment N sink. Nevertheless, potential rates can be compared across studies that have used similar techniques to put the rates that we measured in perspective. The range of average denitrification potential rates (2.1-80.4 nmol N cm^{-3} h^{-1}) across stations that we measured is typical for studies employing similar techniques at different locations in shelf or deep-sea sediments (Trimmer and Engström 2011, Brin et al. 2014). Higher denitrification potential rates have been reported in samples from coastal bays or

estuaries but in general the denitrification potential rates that we measured in shelf sediments are still in the range typically measured in shallower sub-tropical, temperate, or arctic sediments. Measurements of denitrification and anammox potential rates in sediments within ODZs are relatively rare, with one example from the Arabian Sea (Sokoll et al. 2012). Surprisingly, the average anammox potential rates that we measured at two of our shelf stations in the ODZ of 25.1 and 44.2 nmol N cm^{-3} h^{-1} (120 m and 325 m stations, respectively) are higher compared to the range of rates measured in different estuarine, shelf, or deep-sea sediments, including the Arabian Sea (Trimmer and Engström 2011, Sokoll et al. 2012, Brin et al. 2014). The factors contributing to the high anammox potential rates that we measured are not clear but could be related to a combination of factors, including undetectable O_2 and relatively high NO_3^- and NO_2^- concentrations in the overlying water and lack of dense *Thioploca* at these two sites. Average anammox potential rates that we measured from the rest of the stations, including the shelf site with dense *Thioploca*, are in the range reported across other estuarine to deep-sea sediments.

In addition to determining denitrification and anammox potential rates using the type of ^{15}N incubations that we employed, rates of these two processes have been less commonly determined using porewater flux calculations or an intact core isotope pairing technique (Martin and Sayles 2004, Trimmer et al. 2006, Trimmer and Engström 2011). In deeper marine sediments (>100m water depth), incubations with homogenized sediments or whole cores have yielded similar results in terms of *ra* (Trimmer et al. 2013). Across eight stations in Washington Margin sediments with a water depth range of 2,740-3,110 m, the range in *ra* was 12-51% (average 38%) (Engström et al. 2009). In the North Sea, spanning a water depth of 50-2000 m, the range in *ra* was 15-65% (average 33%) (Trimmer and Nichols 2009). Across four stations in in the Arabian Sea with a water depth range of 360-1430 m, *ra* increased with depth from 7% to

40% (average ~20%) (Sokoll et al. 2012). Average *ra* is similar among the Washington Margin, the North Sea, and our study, ~33-38%, but higher than the average in the Arabian Sea. Comparing this relatively small dataset to rates in sediments from Skagerrak indicates that the relatively high *ra* of 79% in the Skagerrak is somewhat unusual, which could be due to relatively high levels of manganese oxides there, which could lead to manganese reducers outcompeting denitrifiers for organic carbon. This may give anammox bacteria a competitive advantage over denitrifiers for NO_2^- at sites with high manganese oxides, in addition to low overall flux of labile organic carbon (Thamdrup and Dalsgaard 2002, Engström et al. 2009). Our study indicates that overall anammox rates are likely to be a quantitatively significant in Peru margin sediments, but not as high as denitrification rates, similar to other studies in deep sediments (Engström et al. 2009, Trimmer and Nicholls 2009, Sokoll et al. 2012).

4.2 Methodological considerations

Applying the stable isotope pairing technique in sediments with *Thioploca* presents some challenges due to intracellular NO_3^- and DNRA. Similarly, the presence of foraminifera could contribute intracellular NO_3^- in our incubations (Glock et al. 2013). It should be noted that our application of the isotope pairing technique does not differentiate between bacterial or foraminiferal denitrification, but rather measures overall denitrification. Leakage or mixing of intracellular NO_3^- into a pool of added $^{15}NO_3^-$ can significantly reduce the atom% ^{15}N of NO_3^- (F_n), leading to significant overestimates of anammox rates, if the effect of intracellular NO_3^- on F_n is not taken into account (Song et al. 2013). In our study, we observed *Thioploca* at two stations (100 m and 325 m), which automatically indicated that intracellular NO_3^- could be an issue. This was confirmed in porewater depth profiles with significantly higher NO_3^- in the

443 porewater than the bottom water, and ^{15}N incubations with high starting NO_3^- concentrations.
444 The F_n values that we calculated based on the standard approach by difference before and after
445 $^{15}NO_3^-$ addition were prone to very large error at these two stations. This resulted in negative
446 anammox rates in some cases and highly variable estimates of *ra* among replicates using the
447 standard equations of Thamdrup and Dalsgaard (2002) for $^{15}NO_3^-$+$^{14}NH_4^+$ additions. To address
448 this issue, others and we have used a modification of the standard isotope pairing equations
449 (Sokoll et al. 2012, Song et al. 2013) relying on $^{15}NH_4^+$+$^{14}NO_3^-$ additions instead of $^{15}NO_3^-$
450 +$^{14}NH_4^+$ additions to determine anammox rates, highlighting the importance of employing both
451 combinations of isotopes (Song et al. 2013). In the other five stations where we did not observe
452 *Thioploca*, anammox rates determined with either isotope combination treatment were similar
453 across all five stations, indicating that intracellular NO_3^- was not a significant factor in our results
454 at these five stations.
455 A second potential issue with applying the stable isotope pairing technique in our
456 samples is the influence of DNRA (Kartal et al. 2006, Song et al. 2016). If DNRA were taking
457 place, $^{15}NH_4^+$ would be produced from added $^{15}NO_3^-$, potentially resulting in $^{15}N^{15}N$ production
458 by anammox and an underestimate of anammox rates in incubations with added $^{15}NO_3^-$+$^{14}NH_4^+$.
459 This was not a factor at our two central shelf stations where we might expect the highest rates of
460 DNRA, as anammox rates at these locations were determined in incubations with added
461 $^{15}NH_4^+$+$^{14}NO_3^-$, not added $^{15}NO_3^-$+$^{14}NH_4^+$. However, DNRA could also influence the isotope
462 labeling of the NH_4^+ pool with added $^{15}NH_4^+$+$^{14}NO_3^-$ by diluting $^{15}NH_4^+$ through conversion of
463 $^{14}NO_3^-$ to $^{14}NH_4^+$. We accounted for potential dilution of $^{15}NH_4^+$ during these incubations in our
464 calculation of anammox rates by accounting for changes in the atom% of ^{15}N-NH_4^+ that may
465 have occurred. Although we did not directly measure DNRA rates in this study, DNRA was not

466 an issue in the determined anammox and denitrification rates at the five other stations, based on
467 similar anammox rates between the two different combinations of isotope additions across these
468 stations. Additional support for the estimated *ra* in shipboard incubations comes from the three
469 stations where we were able to determine NO_3^- and NH_4^+ fluxes based on porewater profiles, as
470 these estimates of *ra* were generally similar to those based on ^{15}N incubations. Directly
471 measuring DNRA rates in these types of incubations would be important in future studies (Song
472 et al. 2016).
473
474 *4.3 Environmental controls on the relative contribution of anammox to rates*
475 Thamdrup and Dalsgaard (2002) predicted a relationship of increasing *ra* with decreasing
476 sediment organic C decomposition rates. However, the trend of decreasing organic C
477 decomposition rates with depth can be variable, depending on the particular study region (e.g.,
478 Hedges and Keil 1995). We could not use porewater oxygen profiles to assess organic C
479 availability based on diffusive oxygen uptake rates across all the stations because three of the
480 seven stations were in the oxygen deficient zone. We measured total organic carbon, but it did
481 not correlate consistently with depth, although there were very high concentrations at the central
482 two shelf stations, reflecting high organic matter deposition and burial in this area. As total
483 organic carbon does not necessarily reflect labile carbon availability at the metabolic level (e.g.,
484 Hedges and Keil 1995), we also examined NH_4^+ production rates as a proxy for organic C
485 decomposition rates, and therefore organic C availability. NH_4^+ production rates were high at the
486 two central shelf stations, indicating high organic C availability at these stations compared to the
487 other five stations. In contrast, NH_4^+ production rates were generally similar at the other five
488 stations, even though they varied widely with depth, suggesting lack of variability in organic C

availability with depth in our other samples, which is not surprising given the large geographic area and varying topography over which we sampled.

Based on the original hypothesis by Thamdrup and Dalsgaard (2002), we would predict that *ra* should be lowest at the station with highest organic C decomposition rates, as indicated by NH_4^+ production rates. In agreement with their hypothesis, we found the lowest *ra* at the 100 m station, where NH_4^+ production rates were the highest. The next highest NH_4^+ production rates were at the 325 m station, while NH_4^+ production rates were relatively low at the rest of the stations. Based on relative differences in NH_4^+ production rates among stations, a second hypothesis based on Thramdup and Dalsgaard (2002) would be that *ra* at the 325 m station would be closer to the low level measured at the 100 m station compared to the rest of the stations. Surprisingly, we did not find this pattern as the *ra* at the 325 m station was ~46%, similar to the other stations with relatively low NH_4^+ production. The jump in *ra* from the 100 m station to the 325 m station was due to both an increase in anammox potential rates and decrease in denitrification potential rates between these two stations. Denitrification potential rates did not show a consistent decrease with labile organic C, based on decreasing NH_4^+ production, suggesting that other factors in addition to labile organic C influenced our results.

Another factor controlling *ra* is likely to be NO_3^- availability. In sediments at different locations with similar labile organic C, greater NO_3^- concentrations in the overlying water or sediment porewater are related to greater *ra*, perhaps because of relieved competition for NO_2^- between denitrifying and anammox bacteria (Rich et al. 2008, Brin et al. 2014, Algar and Vallino 2014). The visual presence of *Thioploca* at two stations in our study may have been a factor contributing to differences in NO_3^- availability in the sediments at these two stations due to the ability of *Thioploca* to transport NO_3^- down into sediments (Huettel et al. 1996). Zopfi et al.

512 (2001) measured NO_3^- microprofiles in intact sediments with dense *Thioploca* mats, and found
513 NO_3^- was not detectable in the porewater in the mat or underlying sediments, suggesting that
514 *Thioploca* retain their intracellular NO_3^- stores efficiently. Porewater NO_3^- concentrations were
515 somewhat higher in sediments with low density *Thioploca* compared to sediments with high
516 density of *Thioploca* (Zopfi et al. 2001), suggesting that there could be differences in NO_3^-
517 availability in sediments with different densities of *Thioploca* in our study. In turn, the density of
518 *Thioploca* is likely related to labile organic C, as patterns of sulfide uptake in *Thioploca* suggest
519 that these microbes are adapted to take advantage of periodically high sulfide concentrations
520 following massive organic matter sedimentation events (Høgslund et al. 2009). Low density
521 *Thioploca* at the 325 m station may have been a remnant of a past organic matter sedimentation
522 event at that location. Perhaps this could have led to greater NO_3^- leakage from *Thioploca* to the
523 surrounding bacterial community in sediments at the 325 m station.
524 Our results of suppressed anammox rates in the *Thioploca* mat at the 100 m station do not
525 necessarily contradict the results of Prokopenko et al. (2013), who found a close association
526 between anammox bacteria and *Thioploca* and significant anammox rates at a station with
527 *Thioploca* off Mexico. Few locations have been examined for the association between anammox
528 and *Thioploca*, so the factors controlling the association are not well understood beyond
529 Prokopenko et al. (2013). The *hzo* qPCR results from this study demonstrate that anammox
530 bacteria were just as abundant at the 100 m station as some of the other stations, suggesting that
531 anammox rates at the 100 m station were not limited by cell numbers of anammox bacteria but
532 rather a physiological mechanism. Based on benthic fluxes and modeling in Peru margin
533 sediments, Sommer et al. (2016) provided evidence that *Thioploca* strongly outcompete
534 denitrifying and anammox bacteria for NO_3^- at locations with thick *Thioploca* mats and

535 extremely high NH_4^+ production rates, much higher than measured in our study. Bohlen et al.
536 (2011) also sampled Peru margin sediments with *Thioploca* mats and NH_4^+ production rates
537 more similar to our study. Based on Bohlen et al. (2011), anammox rates are completely
538 inhibited in sediments with thick *Thioploca* mats, while denitrification rates are still active,
539 which is a pattern similar to our results at the 100 m station. Inhibition of anammox rates due to
540 hydrogen sulfide is also a possible factor (Jensen et al. 2008). However, *Thioploca* are proficient
541 sulfur oxidizers and dissolved H_2S concentrations in intact *Thioploca* mats are generally below
542 detection (Ferdelman et al. 1997), except in some extreme cases (Sommer et al. 2016). To rectify
543 apparently contradictory results between our work and others in terms of the relationship
544 between *Thioploca* and anammox, we propose that the relationship between anammox bacteria
545 and *Thioploca* depends on the density and perhaps physiological condition of *Thioploca* found at
546 a particular site, which would influence the ability of *Thioploca* to compete for NO_3^-. This might
547 explain why we found relatively high rates of anammox in the presence of relatively sparse
548 *Thioploca* at the 325 m station, but almost complete suppression of anammox rates at the 100 m
549 station in the presence of a dense *Thioploca* mat.
550
551 *4.4* Candidatus *Scalindua in marine sediments*
552 From deep sea hydrothermal vents (Byrne et al. 2008) to sediments collected across the
553 equatorial Pacific (Hong et al. 2011), the dominance of *Ca.* Scalindua sequences is consistent in
554 marine sediments. Anammox bacteria have been detected by 16S rDNA sequences in the water
555 column in ODZs in the Eastern Pacific (Hamersley et al. 2007, Galán et al. 2009), the Arabian
556 Sea (Jayakumar et al. 2009, Woebken et al. 2008), and the Namibian upwelling system (Kuypers
557 et al 2005). Sequences with high similarity to those of *Ca.* Scalindua also dominate these

environments. Our study confirms low phylogenetic diversity of anammox bacteria in marine ecosystems (Schmid et al. 2007), with all anammox specific sequences forming a monophyletic cluster with representative sequences of *Ca.* Scalindua. Despite the pattern of dominance of *Ca.* Scalindua in the oceans, small-scale patterns of diversity within this group have been observed. Woeboken et al. (2008) described two major clades of *Ca*. Scalindua in three major ODZs, with phylogenetic groupings (at 98% similarity for 16S rRNA genes) corresponding to different regions, i.e., Peru and the Arabian Sea. Hirsch et al. (2011) found supporting evidence for a deep-sea clade within Scalindua containing representatives from deep-sea hydrothermal vents and a submarine pyroclastic deposit. Spatial differentiation between anammox clades has also been observed at sites distributed across long distances in the equatorial Pacific (Hong et al. 2011).

In the Peru margin sediments, sequences from the sampling stations did not separate into site-specific phylogenetic subclusters, although the number of OTUs (defined at the 98% similarity for 16S rRNA and 96% similarity for *hzo*) exceeded the number of OTUs reported for the water column environments. A single amino acid change in the sequenced *hzo* fragments segregated the majority of the Peru margin anammox community into shelf and deep sediment types (Fig. 6D). While both of these types were part of the same subgroup within the larger *Ca*. Scalindua clade, this could be indicative of a microdiversity pattern that might be of ecological significance in terms of different physiological or kinetic adaptations to changes in pressure or temperature. Although we can only speculate on the functional implications of the amino acid change, examples of single amino acid changes resulting in differences in protein function are not uncommon (Bryan et al. 2000, Gong and Basilico 1990, Joshi et al. 2000).

4.5 Conclusions

Results from our study suggest that anammox is a significant process contributing to N_2 production in Peru margin sediments, overall, with the exception of shallower shelf sediments with *Thioploca* mats. There are challenges to applying the standard isotope pairing technique in sediments with *Thioploca* due primarily to intracellular NO_3^- and possibly DNRA. Under these circumstances, our study further demonstrated the importance of parallel incubations with different combinations of isotopes to determine anammox and denitrification potential rates (Sokoll et al. 2012, Song et al. 2013). Except for the two central shelf stations, NH_4^+ production rates were similar in sediments with large differences in depth, indicative of overall high organic matter deposition in the region and large spatial variability over which we sampled. *ra* was relatively constant in four out of five stations with similar NH_4^+ production rates, consistent with the role of labile organic C flux as a factor controlling *ra*. In the two central shelf stations, with the highest NH_4^+ production rates, there were large differences in *ra* that were not expected based on NH_4^+ production rates alone. We propose that the difference in density of *Thioploca* and perhaps their physiological condition was a factor contributing to differences in *ra* at the two central shelf stations. The molecular data further support the ubiquitous role of anammox bacteria in the genus *Ca.* Scalindua in the marine environment, with an indication of fine-scale patterns in the distribution of diversity between shelf and deep sediments.

Acknowledgements

We thank the crew and science party aboard the R/V Knorr (leg 182-9) for assistance and support. We particularly thank chief scientist Dr. James Moffett at the University of Southern California for his generosity and Dr. Timothy Eglinton at ETH Zurich for leading the multi-

coring effort and providing the %TOC data. This work was supported by the National Science Foundation (NSF) Microbial Biology Postdoctoral Fellowship Program (DBI-0301308 to JJR) and NSF to BBW and AHD (OCE-0647981 to AHD).

References Cited

Algar, C., and Vallino, J. (2014). Predicting microbial nitrate reduction pathways in coastal sediments. Aquat. Microb. Ecol. 71, 223–238. doi:10.3354/ame01678.

Babbin, A. R., Keil, R. G., Devol, A. H., and Ward, B. B. (2014). Organic matter stoichiometry, flux, and oxygen control nitrogen loss in the ocean. Science 344, 406–8. doi:10.1126/science.1248364.

Berelson, W. M., Hammond, D. E., Oneill, D., Xu, X. M., Chin, C., and Zukin, J. (1990). Benthic fluxes and pore water studies from sediments of the central equatorial north Pacific: nutrient diagenesis. Geochim. Cosmochim. Acta 54, 3001–3012.

Bohlen, L., Dale, A. W., Sommer, S., Mosch, T., Hensen, C., Noffke, A., et al. (2011). Benthic nitrogen cycling traversing the Peruvian oxygen minimum zone. Geochim. Cosmochim. Acta 75, 6094–6111.

Boudreau, B. (1997). Diagenetic Models and Their Implementation: Modelling Transport and Reactions in Aquatic Sediments. New York: Springer.

Braman, R. S., and Hendrix, S. A. (1989). Nanogram nitrite and nitrate determination in environmental and biological materials by vanadium (III) reduction with chemiluminescence detection. Anal Chem 61, 2715–2718.

Brin, L. D., Giblin, A. E., and Rich, J. J. (2014). Environmental controls on anammox and denitrification in Southern New England estuarine and shelf sediments. Limnol. Ocean. 59, 851–860.

Broenkow, W. W., and Cline, J. D. (1969). Colorimetric determination of dissolved oxygen at low concentrations. Limnol. Oceanogr. 14, 450–454.

Bryan, G. T., Wu, K.-S., Farrall, L., Jia, Y., Hershey, H. P., McAdams, S. A., et al. (2000). A Single Amino Acid Difference Distinguishes Resistant and Susceptible Alleles of the Rice Blast Resistance Gene Pi-ta. Plant Cell Online 12, 2033–2046.

Byrne, N., Strous, M., Crepeau, V., Kartal, B., Birrien, J.-L., Schmid, M., et al. (2008). Presence and activity of anaerobic ammonium-oxidizing bacteria at deep-sea hydrothermal vents. ISME J 3, 117–123.

636 Christensen, J. P., Murray, J. W., Devol, A. H., and Codispoti, L. A. (1987). Denitrification in
637 continental shelf sediments has major impact on the oceanic nitrogen budget. Global
638 Biogeochem. Cycles 1, 97–116.

639 Dalsgaard, T., Thamdrup, B., Farías, L., and Peter Revsbech, N. (2012). Anammox and
640 denitrification in the oxygen minimum zone of the eastern South Pacific. Limnol.
641 Oceanogr. 57, 1331–1346. doi:10.4319/lo.2012.57.5.1331.

642 Devol, A. H. (1991). Direct measurement of nitrogen gas fluxes from continental shelf
643 sediments. Nature 349, 319–321.

644 DeSantis, T. Z., Hugenholtz, P., Larsen, N., Rojas, M., Brodie, E. L., Keller, K., et al. (2006).
645 Greengenes, a Chimera-Checked 16S rRNA Gene Database and Workbench Compatible
646 with ARB. Appl. Environ. Microbiol. 72, 5069–5072.

647 Engström, P., Dalsgaard, T., Hulth, S., and Aller, R. C. (2005). Anaerobic ammonium oxidation
648 by nitrite (anammox): Implications for N2 production in coastal marine sediments.
649 Geochim. Cosmochim. Acta 69, 2057–2065.

650 Engström, P., Penton, C. R., and Devol, A. H. (2009). Anaerobic ammonium oxidation in deep-
651 sea sediments off the Washington margin. Limnol. Ocean. 54, 1643–1652.

652 Ferdelman, T. G., Lee, C., Pantoja, S., Harder, J., Bebout, B. M., and Fossing, H. (1997). Sulfate
653 reduction and methanogenesis in a *Thioploca*-dominated sediment off the coast of Chile.
654 Geochim. Cosmochim. Acta 61, 3065–3079.

655 Fossing, H., Gallardo, V. A., Jorgensen, B. B., Huttel, M., Nielsen, L. P., Schulz, H., et al.
656 (1995). Concentration and transport of nitrate by the mat-forming sulfur bacterium
657 *Thioploca*. Nature 374, 713–715.

658 Froelich, P. N., Arthur, M. A., Burnett, W. C., Deakin, M., Hensley, V., Jahnke, R., et al. (1988).
659 Early diagenesis of organic matter in Peru continental margin sediments: phosphorite
660 precipitation. Mar. Geol. 80, 309–343.

661 Galloway, J. N., Dentener, F. J., Capone, D. G., Boyer, E. W., Howarth, R. W., Seitzinger, S. P.,
662 et al. (2004). Nitrogen cycles: past, present, and future. Biogeochemistry 70, 153–226.

663 Glock, N., Schönfeld, J., Eisenhauer, A., Hensen, C., Mallon, J., and Sommer, S. (2013). The
664 role of benthic foraminifera in the benthic nitrogen cycle of the Peruvian oxygen
665 minimum zone. Biogeosciences 10, 4767–4783. doi:10.5194/bg-10-4767-2013.

666 Gong, S. S., and Basilico, C. (1990). A mammalian temperature-sensitive mutation affecting G1
667 progression results from a single amino acid substitution in asparagine synthetase.
668 Nucleic Acids Res. 18, 3509.

669 Guindon, S., Dufayard, J., Lefort, V., Anisimova, M., Hordijk, W., and Gascuel, O. (2010). New
670 Algorithms and Methods to Estimate Maximum-Likelihood Phylogenies: Assessing the
671 Performance of PhyML 3.0. Syst. Biol. 59, 307–321.

672 Haeckel, M., Konig, I., Reich, V., Weber, M. E., and Suess, E. (2001). Pore water profiles and
673 numerical modelling of biogeochemical processes in Peru Basin deep-sea sediments.
674 Deep. Res. Part II-Topical Stud. Oceanogr. 48, 3713–3736.

675 Hamersley, M. R., Lavik, G., Woebken, D., Rattray, J. E., Lam, P., Hopmans, E. C., et al.
676 (2007). Anaerobic ammonium oxidation in the Peruvian oxygen minimum zone. Limnol.
677 Oceanogr. 52, 923–933.

678 Hedges, J. I., and Keil, R. G. (1995). Sedimentary organic-matter preservation: an assessment
679 and speculative synthesis. Mar. Chem. 49, 81–115.

680 Henrichs, S. M., and Farrington, J. W. (1984). Peru upwelling region sediments near 15-degrees
681 south. 1. remineralization and accumulation of organic matter. Limnol. Oceanogr. 29, 1–
682 19.

683 Hirsch, M. D., Long, Z. T., and Song, B. (2011). Anammox bacterial diversity in various aquatic
684 ecosystems based on the detection of hydrazine oxidase genes. Microb. Ecol. 61, 264–
685 276.

686 Høgslund, S., Revsbech, N. P., Kuenen, J. G., Jørgensen, B. B., Gallardo, V. A., van de
687 Vossenberg, J., et al. (2009). Physiology and behaviour of marine *Thioploca*. ISME J. 3,
688 647–57. doi:10.1038/ismej.2009.17.

689 Hong, Y.-G., Yin, B., and Zheng, T.-L. (2011). Diversity and abundance of anammox bacterial
690 community in the deep-ocean surface sediment from equatorial Pacific. Appl. Microbiol.
691 Biotechnol. 89, 1233–1241. doi:10.1007/s00253-010-2925-4.

692 Huettel, M., Forster, S., Kloser, S., and Fossing, H. (1996). Vertical migration in the sediment-
693 dwelling sulfur bacteria *Thioploca* spp in overcoming diffusion limitations. Appl.
694 Environ. Microbiol. 62, 1863–1872.

695 Jayakumar, A., Naqvi, S. W. A., and Ward, B. B. (2009). “Distribution and relative
696 quantification of key genes involved in fixed nitrogen loss from the Arabian Sea oxygen
697 minimum zone,” in Indian Ocean Biogeochemical Processes and Ecological Variability,
698 eds. J. D. Wiggert and R. R. Hood (Washington, D. C.: American Geophysical Union),
699 187–203.

700 Jensen, M. M., Kuypers, M., Lavik, G., and Thamdrup, B. (2008). Rates and regulation of
701 anaerobic ammonium oxidation and denitrification in the Black Sea. Limnol. Oceanogr.
702 53, 23–36.

703 Joshi, M. D., Sidhu, G., Pot, I., Brayer, G. D., Withers, S. G., and McIntosh, L. P. (2000).
704 Hydrogen bonding and catalysis: a novel explanation for how a single amino acid
705 substitution can change the pH optimum of a glycosidase. J. Mol. Biol. 299, 255–279.

706 Kartal, B., and Keltjens, J. T. (2016). Anammox Biochemistry : a Tale of Heme c Proteins.
707 Trends Biochem. Sci. 41, 998–1011. doi:10.1016/j.tibs.2016.08.015.

708 Kartal, B., Keltjens, J. T., and Jetten, M. S. M. (2011a). “Metabolism and Genomics of anammox
709 bacteria,” in Nitrification, eds. B. B. Ward, D. J. Arp, and M. G. Klotz (Washington, D.
710 C.: American Society for Microbiology Press), 181–200.

711 Kartal, B., Kuypers, M. M. M., Lavik, G., Schalk, J., den Camp, H., Jetten, M. S. M., et al.
712 (2006). Anammox bacteria disguised as denitrifiers: nitrate reduction to dinitrogen gas
713 via nitrite and ammonium. Environ. Microbiol. 9, 635–642.

714 Kartal, B., Maalcke, W. J., de Almeida, N. M., Cirpus, I., Gloerich, J., Geerts, W., et al. (2011b).
715 Molecular mechanism of anaerobic ammonium oxidation. Nature 479, 127-130.

716 Klotz, M. G., Schmid, M. C., Strous, M., Camp, H. J. M. Den, Jetten, M. S. M., and Hooper, A.
717 B. (2008). Evolution of an octahaem cytochrome c protein family that is key to aerobic
718 and anaerobic ammonia oxidation by bacteria. Env. Microbiol 10, 3150–3163.
719 doi:10.1111/j.1462-2920.2008.01733.x.

720 Koroleff, F. (1983). “Determination of nutrients,” in Methods of Seawater Analysis, ed. K.
721 Grasshoff (Verlag Chemie).

722 Kuypers, M. M. M., Lavik, G., Woebken, D., Schmid, M., Fuchs, B. M., Amann, R., et al.
723 (2005). Massive nitrogen loss from the Benguela upwelling system through anaerobic
724 ammonium oxidation. Proc. Natl. Acad. Sci. U. S. A. 102, 6478–6483.

725 Lam, P., Lavik, G., Jensen, M. M., van de Vossenberg, J., Schmid, M., Woebken, D., et al.
726 (2009). Revising the nitrogen cycle in the Peruvian oxygen minimum zone. Proc. Natl.
727 Acad. Sci. U. S. A. 106, 4752–4757. doi:10.1073/pnas.0812444106.

728 Levin, L., Gutierrez, D., Rathburn, A., Neira, C., Sellanes, J., Munoz, P., et al. (2002). Benthic
729 processes on the Peru margin: a transect across the oxygen minimum zone during the
730 1997-98 El Nino. Prog. Oceanogr. 53, 1–27.

731 Martin, W. R., and Sayles, F. L. (2004). Organic matter cycling in sediments of the continental
732 margin in the northwest Atlantic Ocean. Deep Sea Res. Part I Oceanogr. Res. Pap. 51,
733 457–489.

734 Middelburg, J. J., Soetaert, K., Herman, P. M. J., and Heip, C. H. R. (1996). Denitrification in
735 marine sediments: A model study. Global Biogeochem. Cycles 10, 661–673.

736 Nielsen, L. P. (1992). Denitrification in sediment determined from nitrogen isotope pairing.
737 FEMS Microbiol. Ecol. 86, 357–362.

738 Otte, S., Kuenen, J. G., Nielsen, L. P., Paerl, H. W., Zopfi, J., Schulz, H. N., et al. (1999).
739 Nitrogen, carbon, and sulfur metabolism in natural *Thioploca* samples. Appl. Environ.
740 Microbiol. 65, 3148–3157.

741 Prokopenko, M. G., Hirst, M. B., De Brabandere, L., Lawrence, D. J. P., Berelson, W. M.,
742 Granger, J., et al. (2013). Nitrogen losses in anoxic marine sediments driven by
743 *Thioploca*-anammox bacterial consortia. Nature 500, 194–198.

744 Rich, J. J., Dale, O. R., Song, B., and Ward, B. B. (2008). Anaerobic ammonium oxidation
745 (anammox) in Chesapeake Bay sediments. Microb. Ecol. 55, 311–320.

746 Risgaard-Petersen, N., Langezaal, A. M., Ingvardsen, S., Schmid, M. C., Jetten, M. S. M., Op
747 den Camp, H. J. M., et al. (2006). Evidence for complete denitrification in a benthic
748 foraminifer. Nature 443, 93–96. doi:10.1038/nature05070.

749 Risgaard-Petersen, N., Meyer, R. L., Schmid, M., Jetten, M. S. M., Enrich-Prast, A., Rysgaard,
750 S., et al. (2004). Anaerobic ammonium oxidation in an estuarine sediment. Aquat.
751 Microb. Ecol. 36, 293–304.

752 Rozen, S., and Skaletsky, H. (1999). Primer3 on the WWW for General Users and for Biologist
753 Programmers. Methods Mol. Biol. 132, 365–386.

754 Schloss, P. D., Westcott, S. L., Ryabin, T., Hall, J. R., Hartmann, M., Hollister, E. B., et al.
755 (2009). Introducing mothur: Open-Source, Platform-Independent, Community-Supported
756 Software for Describing and Comparing Microbial Communities. Appl. Environ.
757 Microbiol. 75, 7537–7541.

758 Schmid, M. C., Hooper, A. B., Klotz, M. G., Woebken, D., Lam, P., Kuypers, M. M. M., et al.
759 (2008). Environmental detection of octahaem cytochrome c hydroxylamine/hydrazine
760 oxidoreductase genes of aerobic and anaerobic ammonium-oxidizing bacteria. Environ.
761 Microbiol. 10, 3140–3149.

762 Schmid, M. C., Maas, B., Dapena, A., de Pas-Schoonen, K. V, de Vossenberg, J. V, Kartal, B., et
763 al. (2005). Biomarkers for in situ detection of anaerobic ammonium-oxidizing
764 (anammox) bacteria. Appl. Environ. Microbiol. 71, 1677–1684.

765 Schmid, M. C., Risgaard-Petersen, N., van de Vossenberg, J., Kuypers, M. M. M., Lavik, G.,
766 Petersen, J., et al. (2007). Anaerobic ammonium-oxidizing bacteria in marine
767 environments: widespread occurrence but low diversity. Environ. Microbiol. 9, 1476–
768 1484.

769 Schulz, H. N., Jorgensen, B. B., Fossing, H. A., and Ramsing, N. B. (1996). Community
770 structure of filamentous, sheath-building sulfur bacteria, *Thioploca* spp, off the coast of
771 Chile. Appl. Environ. Microbiol. 62, 1855–1862.

772 Sokoll, S., Holtappels, M., Lam, P., Collins, G., Schlüter, M., Lavik, G., et al. (2012). Benthic
773 nitrogen loss in the Arabian Sea off Pakistan. Front. Microbiol. 3, 1–17.
774 doi:10.3389/fmicb.2012.00395.

775 Sommer, S., Gier, J., Treude, T., Lomnitz, U., Dengler, M., Cardich, J., et al. (2016). Depletion
776 of oxygen, nitrate and nitrite in the Peruvian oxygen minimum zone cause an imbalance
777 of benthic nitrogen fluxes. Deep. Res. Part I 112, 113–122.
778 doi:10.1016/j.dsr.2016.03.001.

779 Song, G. D., Liu, S. M., Kuypers, M. M. M., and Lavik, G. (2016). Application of the isotope
780 pairing technique in sediments where anammox, denitrification, and dissimilatory nitrate

781 reduction to ammonium coexist. Limnol. Oceanogr. Methods 14, 801–815.
782 doi:10.1002/lom3.10127.

783 Song, G. D., Liu, S. M., Marchant, H., Kuypers, M. M. M., and Lavik, G. (2013). Anammox,
784 denitrification and dissimilatory nitrate reduction to ammonium in the East China Sea
785 sediment. Biogeosciences 10, 6851–6864. doi:10.5194/bg-10-6851-2013.

786 Sonthiphand, P., Hall, M. W., and Neufeld, J. D. (2014). Biogeography of anaerobic ammonia-
787 oxidizing (anammox) bacteria. Front. Microbiol. 5, 1–14.
788 doi:10.3389/fmicb.2014.00399.

789 Strickland, J. D., and Parsons, T. R. (1972). A practical handbook of seawater analysis. Fish.
790 Res. board Canada 167, 1–311.

791 Thamdrup, B., and Canfield, D. E. (1996). Pathways of carbon oxidation in continental margin
792 sediments off central Chile. Limnol. Oceanogr. 41, 1629–1650.

793 Thamdrup, B., and Dalsgaard, T. (2000). The fate of ammonium in anoxic manganese oxide-rich
794 marine sediment. Geochim. Cosmochim. Acta 64, 4157–4164.

795 Thamdrup, B., and Dalsgaard, T. (2002). Production of N_2 through anaerobic ammonium
796 oxidation coupled to nitrate reduction in marine sediments. Appl. Environ. Microbiol. 68,
797 1312–1318.

798 Trimmer, M., and Engström, P. (2011). “Distribution, activity, and ecology of anammox bacteria
799 in aquatic environments,” in Nitrification, eds. B. B. Ward, D. J. Arp, and M. G. Klotz
800 (Washington, D. C.: American Society for Microbiology Press), 201–235.

801 Trimmer, M., Engström, P., Thamdrup, B., Trimmer, M., and Engström, P. (2013). Stark
802 Contrast in Denitrification and Anammox across the Deep Norwegian Trench in the
803 Skagerrak. Appl. Environ. Microbiol. 79, 7381–7389. doi:10.1128/AEM.01970-13.

804 Trimmer, M., and Nicholls, J. C. (2009). Production of nitrogen gas via anammox and
805 denitrification in intact sediment cores along a continental shelf to slope transect in the
806 North Atlantic. Limnol. Oceanogr. 54, 577–589.

807 Trimmer, M., Risgaard-Petersen, N., Nicholls, J. C., and Engström, P. (2006). Direct
808 measurement of anaerobic ammonium oxidation (anammox) and denitrification in intact
809 sediment cores. Mar. Ecol. Prog. Ser. 326, 37–47.

810 Ullman, W. J., and Aller, R. C. (1982). Diffusion-Coefficients in Nearshore Marine-Sediments.
811 Limnol. Ocean. 27, 552–556.

812 Ward, B. B., Devol, A. H., Rich, J. J., Chang, B. X., Bulow, S. E., Naik, H., et al. (2009).
813 Denitrification as the dominant nitrogen loss process in the Arabian Sea. Nature 461, 78–
814 81.

Woebken, D., Lam, P., Kuypers, M. M. M., Naqvi, S. W. A., Kartal, B., Strous, M., et al. (2008). A microdiversity study of anammox bacteria reveals a novel Candidatus Scalindua phylotype in marine oxygen minimum zones. Environ. Microbiol. 10, 3106–3119.

Zopfi, J., Kjaer, T., Nielsen, L. P., and Jorgensen, B. B. (2001). Ecology of *Thioploca* spp.: Nitrate and sulfur storage in relation to chemical microgradients and influence of *Thioploca* spp. on the sedimentary nitrogen cycle. Appl. Environ. Microbiol. 67, 5530–5537.

Zumft, W. G. (1997). Cell biology and molecular basis of denitrification. Microbiol. Mol. Biol. Rev. 61, 533–616.

Figure Legend

Figure 1. Location and corresponding water column depth of each station (meters). Bathymetry lines include 500 m and 1000 m isobaths, then 1000 m increments thereafter, down to a depth of 6000 m.

Figure 2. Porewater depth profiles of NO_3^-+NO_2^- and NH_4^+ concentrations at the multi-core stations [note: Profiles were not measured at stations MC2 (125 m) and MC9 (1512 m]. There are different scales for NO_3^-+NO_2^- and NH_4^+, corresponding to higher concentrations at the two shelf stations (MC5 and MC12).

Figure 3. Dissolved inorganic N and ^{15}N-N_2 production in incubations of homogenized sediments from the Peru margin shelf stations. Concentrations of NO_3^-, NO_2^-, and dissolved NH_4^+ in the porewater of sediments with added NO_3^- and NH_4^+ (top row), and production of ^{15}N-N_2 in sediments with different combinations of added $^{14/15}N$ (bottom three rows) are shown (average ± SE, n=3). The panels are organized in columns, one column for each station (identified by depth), and rows, one row for each N addition (identified at right). Note that the scale for nmol N cm^{-3} differs among rows.

Figure 4. Same as in Figure 3, except for the Peru margin slope and rise stations.

Figure 5. Average (± SE, n=3) anammox rates in homogenized sediments with added $^{15}NH_4^+$+$^{14}NO_3^-$ (x-axis) or $^{15}NO_3^-$+$^{14}NH_4^+$ (y-axis) from five stations in the Peru margin. The mean slope of the line is not statistically different from one (p=0.7954). Note: The two stations with visible evidence of *Thioploca* (i.e., 100 m and 325 m) are not shown, as anammox rates were determined with added $^{15}NH_4^+$+$^{14}NO_3^-$ only due to the influence of intracellular NO_3^- during incubations in $^{15}NO_3^-$+$^{14}NH_4^+$ additions.

Figure 6. Average of measured parameters and water column depth at each station in the study: (A) %TOC or qPCR *hzo* counts, (B) Upward NH_4^+ flux based on porewater depth profiles (mmol NH_4^+ m^{-2} d^{-1}) or dissolved NH_4^+ production rates measured in vial incubations, corresponding to NH_4^+ released during decomposition of organic matter (nmol NH_4^+ cm^{-3} h^{-1}), (C) anammox or denitrification potential rates (nmol N cm^{-3} h^{-1}) or *ra* (%), and (D) relative abundance of the two most abundant *hzo* genotypes in clone libraries.

Figure 7. Maximum-likelihood phylogenetic tree of 16S rRNA sequences. Sequences representing clone library OTUs from this study are bolded. Bolded leaf labels include the name of the OTU, the total number of clone sequences represented by that OTU in parentheses, followed by a list of what sites are represented within each OTU. The number of sequences per site is in parentheses. The tree was rooted with a 16S rDNA sequence from the Deltaproteobacterium *Desulfobulbus* sp.(GenBank: DSU85473). This outgroup was removed to improve branch length resolution. Scale bar units represent 0.1 nucleotide substitutions per site. Bootstrap support of >70% (white circles) and >90% (black circles) are shown.

Figure 8. Maximum-likelihood phylogenetic tree of Hzo amino acid sequences. Sequences representing OTUs from this study are bolded. Bolded labels include the name of the OTU, the

total number of clone sequences represented by that OTU in parentheses, followed by a list of what stations are represented within each OTU, and the number of sequences per site. The tree was rooted with the Hzo group 2 sequence of *Ca.* Scalindua (GenBank: CAJ7180) as an outgroup (not shown). Scale bar units represent 0.05 amino acid substitutions per site. Bootstrap support of >70% (white circles) and >90% (black circles) are shown.

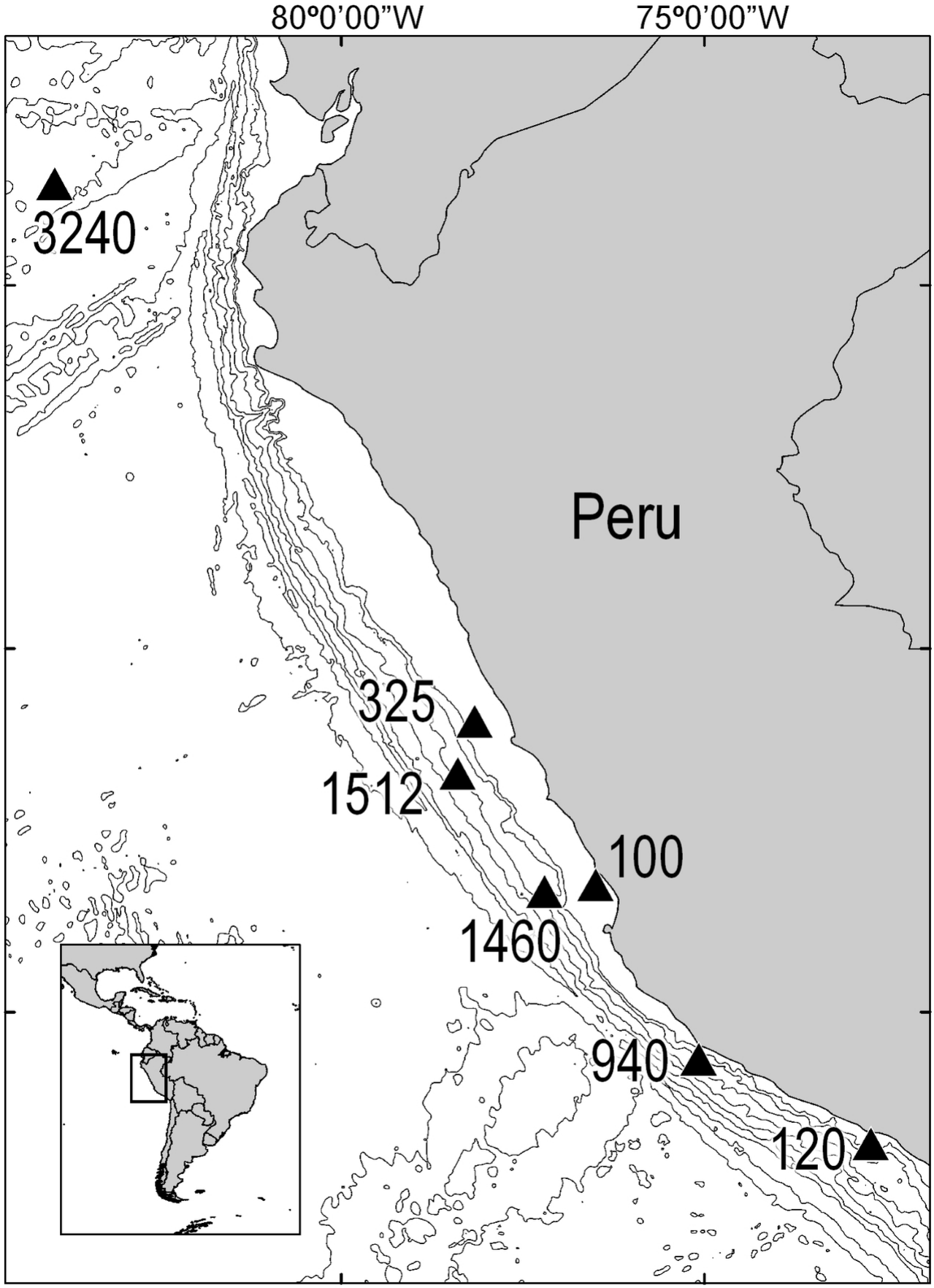
80°0'00"W
75°0'00"W
5°0'00"S
10°0'00"S
15°0'00"S
Peru
3240
325
1512
100
1460
940
120

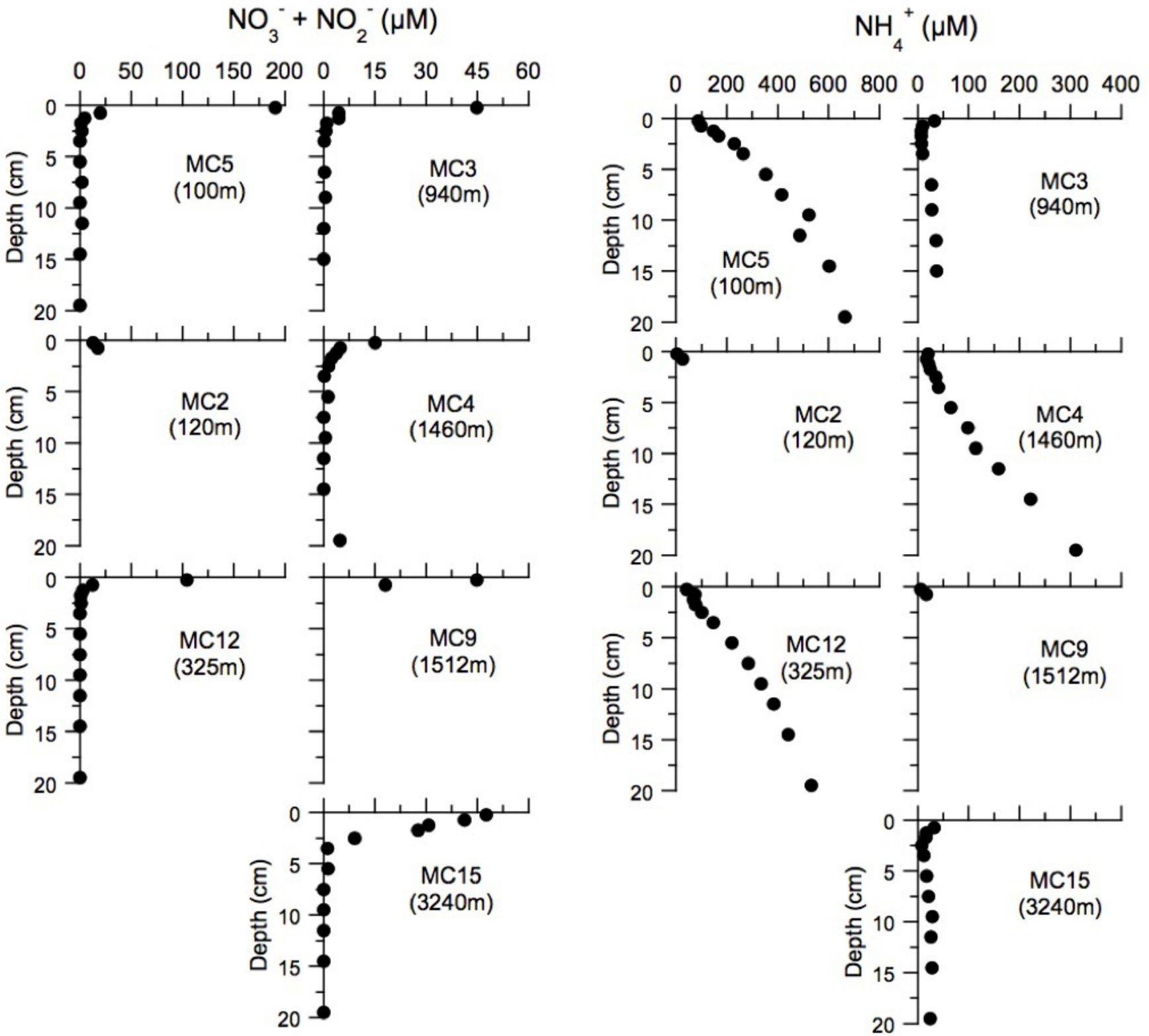
$NO_3^- + NO_2^-$ (μM)
0 50 100 150 200
0 15 30 45 60
NH_4^+ (μM)
0 200 400 600 800
0 100 200 300 400
Depth (cm)
0 5 10 15 20
MC5 (100m)
MC3 (940m)
MC2 (120m)
MC4 (1460m)
MC12 (325m)
MC9 (1512m)
MC15 (3240m)

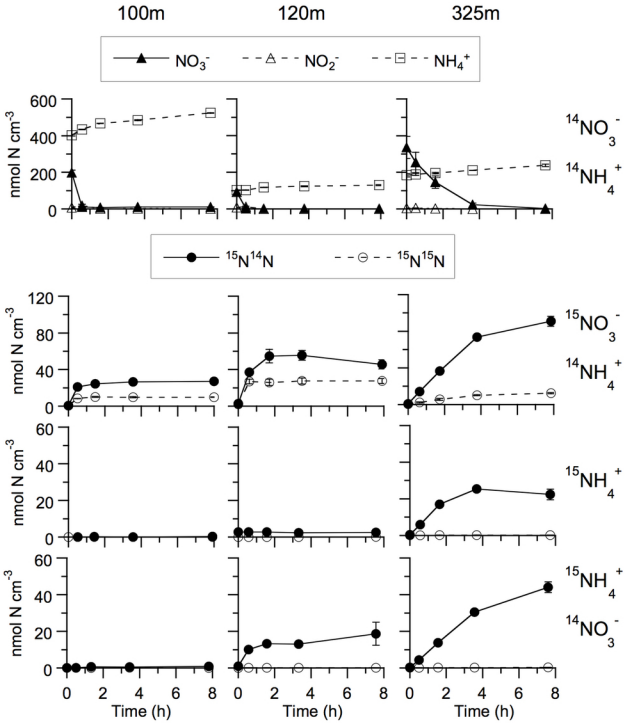
100m
120m
325m
NO3-
NO2-
NH4+
nmol N cm-3
14NO3-
14NH4+
15N14N
15N15N
15NO3-
15NH4+
14NO3-
Time (h)

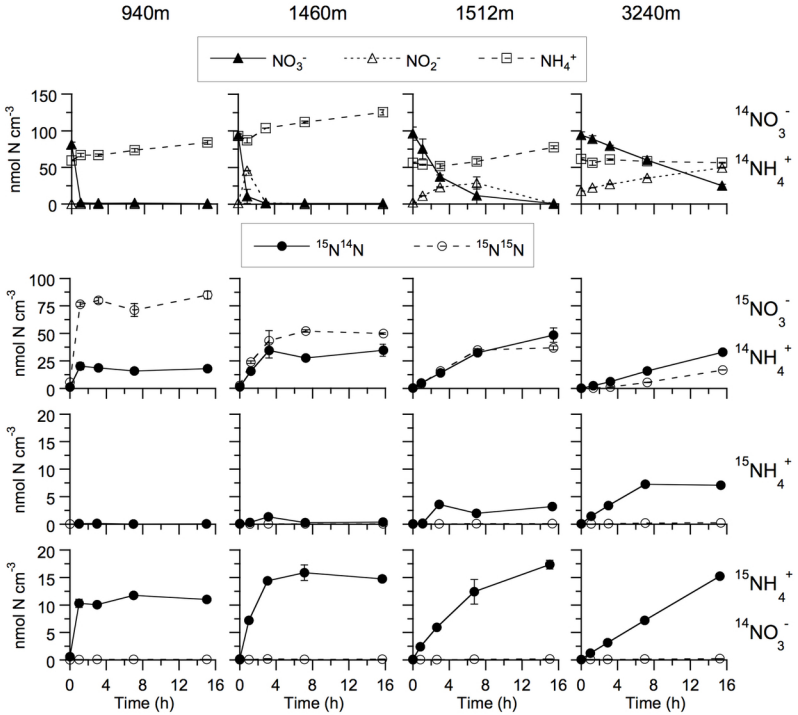
940m
1460m
1512m
3240m
NO3-
NO2-
NH4+
nmol N cm-3
14NO3-
14NH4+
15N14N
15N15N
15NO3-
15NH4+
Time (h)

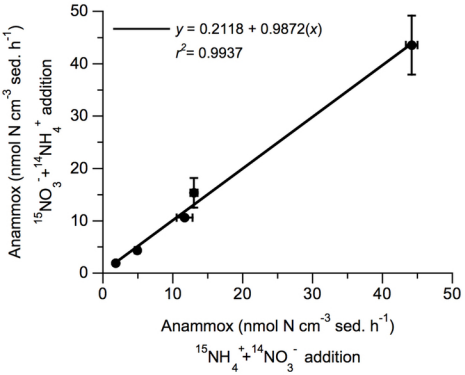
y = 0.2118 + 0.9872(x)
r2= 0.9937
Anammox (nmol N cm-3 sed. h-1)
15NO3-+14NH4+ addition
Anammox (nmol N cm-3 sed. h-1)
15NH4++14NO3- addition
0
10
20
30
40
50

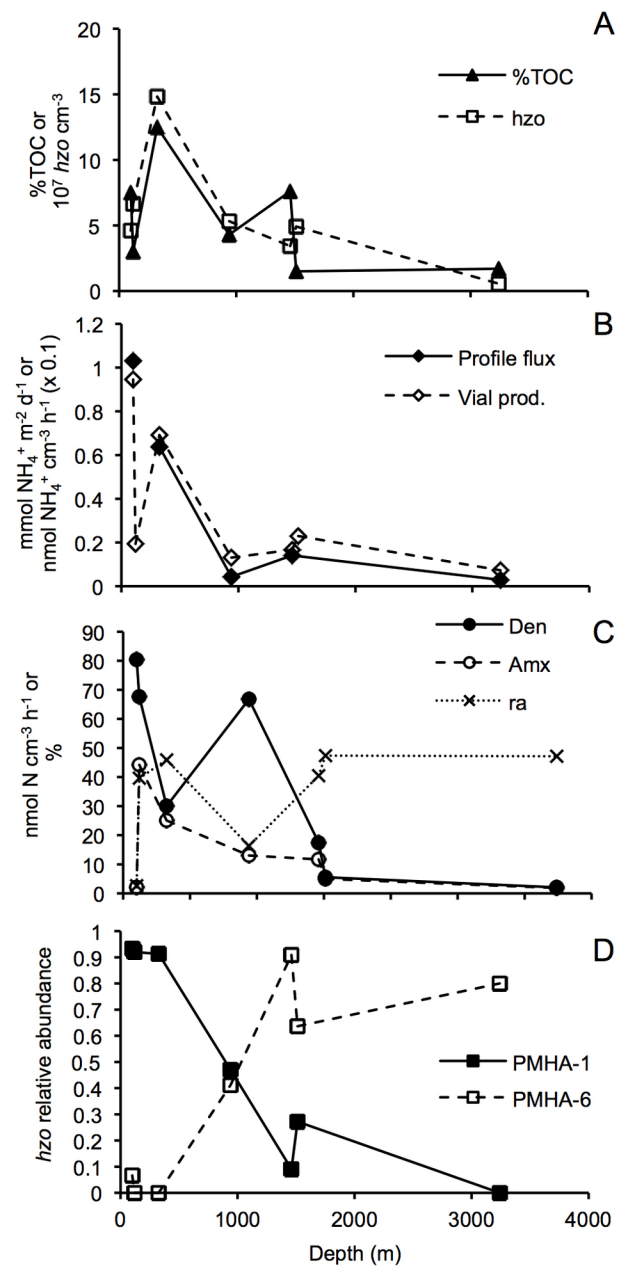
A
%TOC or
10^7 hzo cm^-3
%TOC
hzo
B
mmol NH4+ m-2 d-1 or
nmol NH4+ cm-3 h-1 (x 0.1)
Profile flux
Vial prod.
C
nmol N cm-3 h-1 or
%
Den
Amx
ra
D
hzo relative abundance
PMHA-1
PMHA-6
Depth (m)

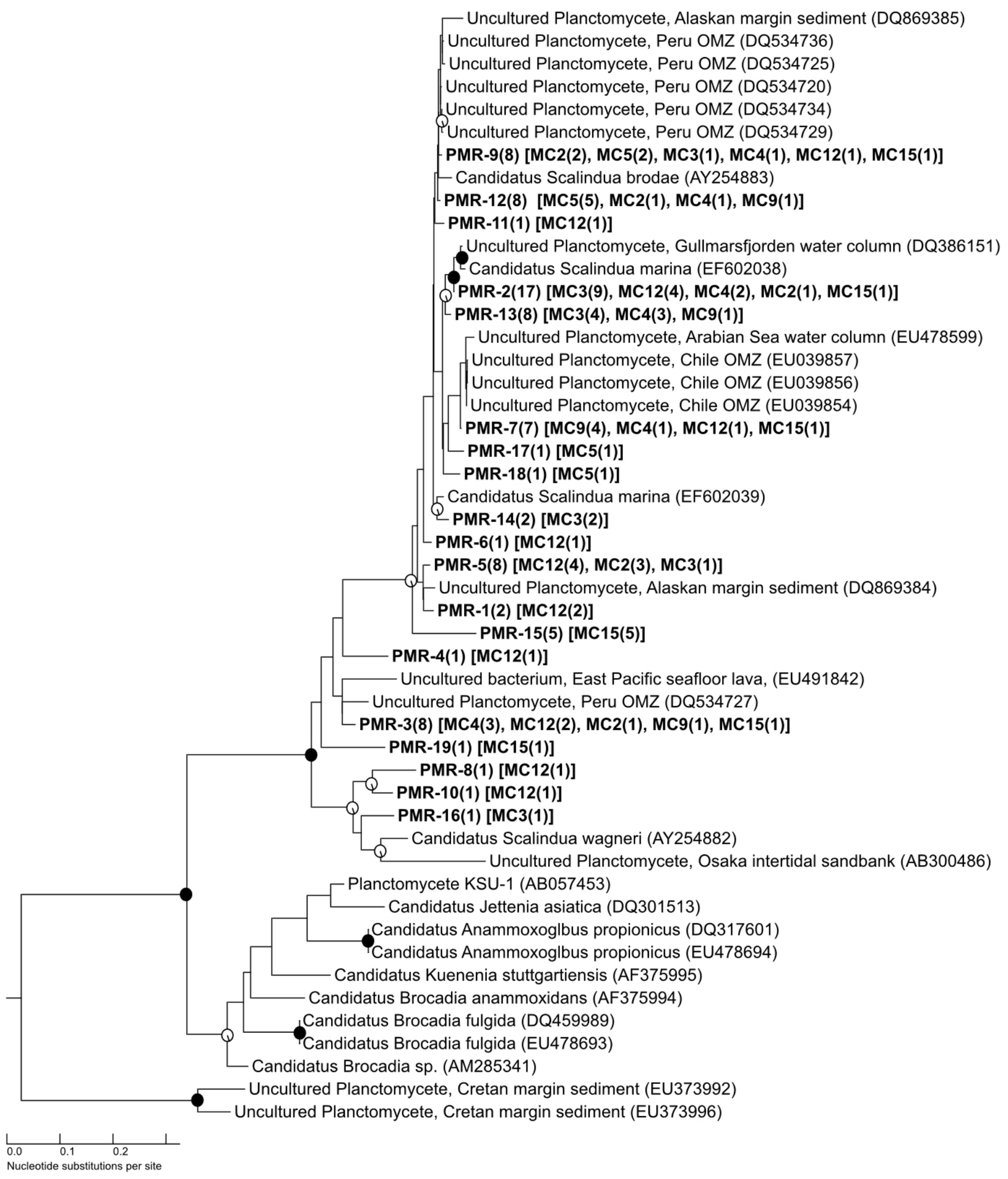
Uncultured Planctomycete, Alaskan margin sediment (DQ869385)
Uncultured Planctomycete, Peru OMZ (DQ534736)
Uncultured Planctomycete, Peru OMZ (DQ534725)
Uncultured Planctomycete, Peru OMZ (DQ534720)
Uncultured Planctomycete, Peru OMZ (DQ534734)
Uncultured Planctomycete, Peru OMZ (DQ534729)
PMR-9(8) [MC2(2), MC5(2), MC3(1), MC4(1), MC12(1), MC15(1)]
Candidatus Scalindua brodae (AY254883)
PMR-12(8) [MC5(5), MC2(1), MC4(1), MC9(1)]
PMR-11(1) [MC12(1)]
Uncultured Planctomycete, Gullmarsfjorden water column (DQ386151)
Candidatus Scalindua marina (EF602038)
PMR-2(17) [MC3(9), MC12(4), MC4(2), MC2(1), MC15(1)]
PMR-13(8) [MC3(4), MC4(3), MC9(1)]
Uncultured Planctomycete, Arabian Sea water column (EU478599)
Uncultured Planctomycete, Chile OMZ (EU039857)
Uncultured Planctomycete, Chile OMZ (EU039856)
Uncultured Planctomycete, Chile OMZ (EU039854)
PMR-7(7) [MC9(4), MC4(1), MC12(1), MC15(1)]
PMR-17(1) [MC5(1)]
PMR-18(1) [MC5(1)]
Candidatus Scalindua marina (EF602039)
PMR-14(2) [MC3(2)]
PMR-6(1) [MC12(1)]
PMR-5(8) [MC12(4), MC2(3), MC3(1)]
Uncultured Planctomycete, Alaskan margin sediment (DQ869384)
PMR-1(2) [MC12(2)]
PMR-15(5) [MC15(5)]
PMR-4(1) [MC12(1)]
Uncultured bacterium, East Pacific seafloor lava, (EU491842)
Uncultured Planctomycete, Peru OMZ (DQ534727)
PMR-3(8) [MC4(3), MC12(2), MC2(1), MC9(1), MC15(1)]
PMR-19(1) [MC15(1)]
PMR-8(1) [MC12(1)]
PMR-10(1) [MC12(1)]
PMR-16(1) [MC3(1)]
Candidatus Scalindua wagneri (AY254882)
Uncultured Planctomycete, Osaka intertidal sandbank (AB300486)
Planctomycete KSU-1 (AB057453)
Candidatus Jettenia asiatica (DQ301513)
Candidatus Anammoxoglbus propionicus (DQ317601)
Candidatus Anammoxoglbus propionicus (EU478694)
Candidatus Kuenenia stuttgartiensis (AF375995)
Candidatus Brocadia anammoxidans (AF375994)
Candidatus Brocadia fulgida (DQ459989)
Candidatus Brocadia fulgida (EU478693)
Candidatus Brocadia sp. (AM285341)
Uncultured Planctomycete, Cretan margin sediment (EU373992)
Uncultured Planctomycete, Cretan margin sediment (EU373996)
0.0
0.1
0.2
Nucleotide substitutions per site

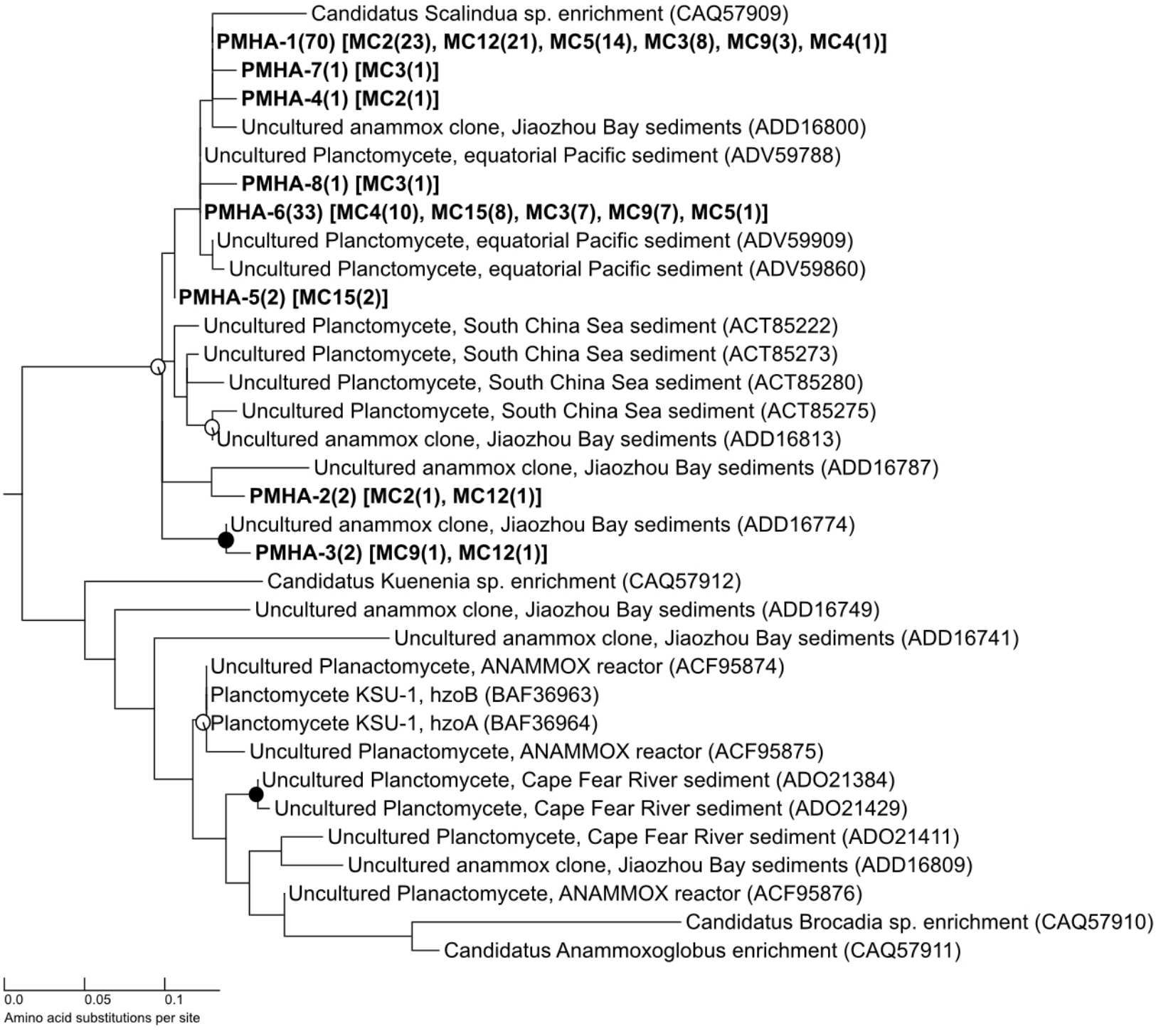
Candidatus Scalindua sp. enrichment (CAQ57909)
PMHA-1(70) [MC2(23), MC12(21), MC5(14), MC3(8), MC9(3), MC4(1)]
PMHA-7(1) [MC3(1)]
PMHA-4(1) [MC2(1)]
Uncultured anammox clone, Jiaozhou Bay sediments (ADD16800)
Uncultured Planctomycete, equatorial Pacific sediment (ADV59788)
PMHA-8(1) [MC3(1)]
PMHA-6(33) [MC4(10), MC15(8), MC3(7), MC9(7), MC5(1)]
Uncultured Planctomycete, equatorial Pacific sediment (ADV59909)
Uncultured Planctomycete, equatorial Pacific sediment (ADV59860)
PMHA-5(2) [MC15(2)]
Uncultured Planctomycete, South China Sea sediment (ACT85222)
Uncultured Planctomycete, South China Sea sediment (ACT85273)
Uncultured Planctomycete, South China Sea sediment (ACT85280)
Uncultured Planctomycete, South China Sea sediment (ACT85275)
Uncultured anammox clone, Jiaozhou Bay sediments (ADD16813)
Uncultured anammox clone, Jiaozhou Bay sediments (ADD16787)
PMHA-2(2) [MC2(1), MC12(1)]
Uncultured anammox clone, Jiaozhou Bay sediments (ADD16774)
PMHA-3(2) [MC9(1), MC12(1)]
Candidatus Kuenenia sp. enrichment (CAQ57912)
Uncultured anammox clone, Jiaozhou Bay sediments (ADD16749)
Uncultured anammox clone, Jiaozhou Bay sediments (ADD16741)
Uncultured Planactomycete, ANAMMOX reactor (ACF95874)
Planctomycete KSU-1, hzoB (BAF36963)
Planctomycete KSU-1, hzoA (BAF36964)
Uncultured Planactomycete, ANAMMOX reactor (ACF95875)
Uncultured Planctomycete, Cape Fear River sediment (ADO21384)
Uncultured Planctomycete, Cape Fear River sediment (ADO21429)
Uncultured Planctomycete, Cape Fear River sediment (ADO21411)
Uncultured anammox clone, Jiaozhou Bay sediments (ADD16809)
Uncultured Planactomycete, ANAMMOX reactor (ACF95876)
Candidatus Brocadia sp. enrichment (CAQ57910)
Candidatus Anammoxoglobus enrichment (CAQ57911)
0.0
0.05
0.1
Amino acid substitutions per site

Table 1. Multi-core station name, location, water depth, and bottom water characteristics.

Station	Latitude	Longitude	Depth (m)	Temperature (˚C)	O_2 (µM)	NO_3^- (µM)	NO_2^- (µM)
Shelf							
MC5	13˚15.00’ S	76˚30.00’ W	100	13.2	<2*	26.1	2.0
MC2	16˚48.83’ S	72˚42.88’ W	120	12.3	<2	ND√	ND
MC12	10˚60.00’ S	78˚10.00’ W	325	10.5	<2	29.7	1.2
Slope							
MC3	15˚38.93’ S	75˚04.98’ W	940	4.6	65.1	43.3	<0.01
MC4	13˚20.63’ S	77˚12.16’ W	1460	3.2	67.1	41.9	<0.01
MC9	11˚43.05’ S	78˚23.93’ W	1512	2.9	71.8	42.4	<0.01
Rise							
MC15	3˚36.23’ S	83˚56.88’ W	3240	1.8	112.5	37.1	<0.01

*O_2 concentration was at or below the detection limit of the sensor of ~2 µM.
√ND, not determined.

Table 2. Multi-core sediment characteristics. The $NO_3^-+NO_2^-$ flux is downward and NH_4^+ flux is upward based on porewater depth profiles.

Station	Depth (m)	*Thioploca* mat	O_2 penetration depth (cm)	%TOC	$NO_3^-+NO_2^-$ flux (mmol m^{-2} d^{-1})	NH_4^+ flux (mmol m^{-2} d^{-1})	Porewater flux *ra* (%)[#]
Shelf							
MC5	100	Yes	ND[*]	7.5	NC[†]	1.031	ND
MC2	120	No	ND	3.0	ND	ND	ND
MC12	325	Sparse	ND	12.5	NC	0.638	ND
Slope							
MC3	940	No	0.5	4.3	0.672	0.043	12.1
MC4	1460	No	0.7	7.6	0.499	0.141	44.0
MC9	1512	No	0.8	1.5	ND	ND	ND
Rise							
MC15	3240	No	1.5	1.7	0.148	0.029	32.9

[*]ND=Not determined.

[†]NC=Not calculated because of intracellular nitrate release during core slicing and centrifugation.

[#]This is the relative anammox rate based on porewater fluxes, $ra = 100(2A/(A+N))$, where A is upward NH_4^+ flux and N is the downward NO_3^- flux.

Table 3. Potential rates (average ± standard deviation, n=3) determined in shipboard ^{15}N incubations of homogenized sediments and *hzo* copy number.

Station	Depth (m)	Denitrif. (nmol N cm^{-3} h^{-1})	Anammox (nmol N cm^{-3} h^{-1})	*ra*	Dissolved NH_4^+ production (nmol N cm^{-3} h^{-1})	*hzo* (copies cm^{-3} $\times 10^7$)
Shelf						
MC5	100	80.4 ± 3.8	2.2 ± 1.3	2.6 ± 1.6	9.5 ± 0.6	4.6 ± 0.7
MC2	120	67.6 ± 4.8	44.2 ± 1.5	39.6 ± 2.3	1.9 ± 0.8	6.6 ± 0.6
MC12	325	30.0 ± 6.5	25.1 ± 1.7	45.9 ± 7.1	6.9 ± 2.9	14.8 ± 3.7
Slope						
MC3	940	66.8 ± 2.9	13.0 ± 0.9	16.3 ± 0.8	1.3 ± 0.4	5.3 ± 0.7
MC4	1460	17.4 ± 3.4	11.7 ± 2.0	40.4 ± 8.8	1.7 ± 0.6	3.4*
MC9	1512	5.5 ± 1.0	5.0 ± 0.5	47.4 ± 7.2	2.3 ± 0.4	4.9 ± 0.2
Rise						
MC15	3240	2.1 ± 0.1	1.8 ± 0.1	47.2 ± 3.2	0.6 ± 0.1	0.6 ± 0.1

*n=1 qPCR reaction for MC4, due to undetectable DNA template concentration in two out of three samples corresponding to this station.